Petroleum Science 21 (2024) 3517–3534

Contents lists available at ScienceDirect

Petroleum Science

journal homepage: www.keaipublishing.com/en/journals/petroleum-science

Original Paper

Optimal depth of in-situ pressure-preserved coring in coal seams considering roadway excavation and drilling disturbance

Peng-Fei Cui [a, b], De-Lei Shang [a, b, c, *], Peng Chu [a, b], Ju Li [d], Da-Li Sun [e], Tian-Yu Wang [c], Ming-Zhong Gao [a, b, c], He-Ping Xie [a, b, c]

[a] State Key Laboratory of Intelligent Construction and Healthy Operation and Maintenance of Deep Underground Engineering, Institute of Deep Earth Sciences and Green Energy, Shenzhen University, Shenzhen, 518060, Guangdong, China
[b] Guangdong Provincial Key Laboratory of Deep Earth Sciences and Geothermal Energy Exploitation and Utilization, Shenzhen Key Laboratory of Deep Underground Engineering Sciences and Green Energy, College of Civil and Transportation Engineering, Shenzhen University, Shenzhen, 518060, Guangdong, China
[c] State Key Laboratory of Hydraulics and Mountain River Engineering, Sichuan University, Chengdu, 610065, Sichuan, China
[d] School of Mechanical Engineering, Sichuan University, Chengdu, 610065, Sichuan, China
[e] Jinshi Drilltech Co., Ltd., Tangshan, 063004, Hebei, China

ARTICLE INFO

Article history:
Received 6 August 2023
Received in revised form
16 May 2024
Accepted 21 May 2024
Available online 23 May 2024

Edited by Jia-Jia Fei

Keywords:
In-situ fidelity coring
In-situ pressure preserved coring
Gas content
Drilling disturbance
Coring depth
Excavation damage zone

ABSTRACT

Using pressure-preserved coring technique to determine in-situ gas content provides a more precise assessment of gas resource reserves and safeguard of mining safety in coal seams. How coring technique and depth affect the determination of gas content is unclear due to borehole zoning rupture caused by roadway excavation and drilling disturbance. To this end, a proposed coupling model of stress distribution and gas migration was simulated and validated by FLAC^{3D} and COMSOL Multiphysics considering superposition effects of roadway excavation and drilling disturbance. The findings indicate that the roadway surrounding rock displays distinct zoning features including stress relief zone, stress concentration zone that is composed of plastic zone, elastic zone, and original stress zone; and the broken situations depending on the borehole peeping are consistent with the corresponding simulation results. On this basis, this study proposes a set of drilling coring depth calculation and prediction model for the gas desorption affected area under engineering disturbance. Optimal depth of coring drilling is not only approach to the in-situ coal bulk, but also can get the balance of the drilling workload and cost controlling. According to the typical mine site geological conditions and the numerical simulation results in this study, if the roadway excavation time is ~1 year, it is recommended that the pressure-preserved coring depth should be greater than 17 m.

1. Introduction

The in-situ coal seams show the characteristics of “high stress, high geothermal temperature, and high pore pressure”, and are accompanied by a series of changes such as soft coal and increasing in gas content. These changes can cause a series of primary and secondary disasters more easily such as outburst and coal seam gas explosion (He et al., 2005; Xie et al., 2020, 2021). Gas content is a critical parameter for preventing gas disasters and accurately evaluating coal seam gas resource reserves. Numerous scholars have conducted extensive research on determining coal seam gas content. At present, there are two methods to determine the gas content, i.e., the direct method & indirect method (Xue and Yuan, 2017). The direct method usually collects cuttings by a canister at the outlet of drilling borehole and gets the gas contents of the coal samples. The Langmuir formula is utilized in the indirect approach to determine the gas content of a coal seam by considering the gas pressure and adsorption constants. In addition, the logging and drilling information is also employed to estimate the gas content in exploration of surface coalbed methane (Wang et al., 2017).

* Corresponding author. State Key Laboratory of Intelligent Construction and Healthy Operation and Maintenance of Deep Underground Engineering, Institute of Deep Earth Sciences and Green Energy, Shenzhen University, Shenzhen, 518060, Guangdong, China.
E-mail address: sdl18@tsinghua.org.cn (D.-L. Shang).

https://doi.org/10.1016/j.petsci.2024.05.014

In terms of the direct method, the coring depth can affect the determination of gas content. On-site coring shows that different coring depths mean different gas desorption time of collecting samples, as shown in Fig. 1. In other words, if a representative undisturbed coal sample needs to be collected, different coring techniques may correspond to different optimal sampling depths; optimal sampling depth means that if the sampling depth is less than a certain depth, then the collecting samples cannot represent the undisturbed horizon at this point. Optimal depth of coring drilling is not only approach to the in-situ coal bulk, but also can get the balance of the drilling workload and cost controlling. However, there are, currently, few reports on how the drilling depth of coring effects on the determination of the gas content. Only in the GB/T 23250 "Method for Direct Determination of Coal Seam Gas Content Underground" stipulated that the coring depth in the mining face should not be < 12 m during the determination of the gas content of coal samples, as shown in Fig. 1, the left dotted line; which, actually, cannot be suitable for all the coring methods. When the coring depth is greater than 50 m, as shown in Fig. 1, the right dotted line, the data of the gas content become random. Thus, to collect more accurate in-situ gas content in the region out of the excavation damage zone, different coal seams or working faces should set up different coring depths.

The method or technique of coring can also affect the determination of gas content. On-site coring shows that different coring techniques mean different sealing methods of collecting samples, as shown in Fig. 1. For open-type coring techniques, such as core tube sampling, outlet sampling, and reverse circulation drilling sampling, the deeper the drilling, the longer exposure time and the greater the desorption gas loss of the sample, as shown in Fig. 1 (data from previous studies (Jing, 2015; Zhang, 2021; Wang et al., 2013; Wang et al., 2020; Zheng et al., 2015; Zhang, 2019; Kang, 2017). Sealing-type coring, such as the in-situ pressure and gas maintaining coring with Mouhe square cover flap valve (Gao et al., 2021), sealed coring with ball valve (Jing, 2015; Sun et al., 2020), can not only avoid or reduce exposure time of the sample in the borehole, but also make the sampling position more accurate.

The direct method has higher accuracy because of its directly to determine gas content, which is based on the industrial standard for coalbed methane content determination in the United States derived from the USBM method proposed by Bertard. It includes estimating the amount of lost gas, the amount of natural desorbed gas before crushing, the amount of naturally desorbed gas after crushing, and the amount of non-desorbable gas under normal pressure. However, considering the traditional method of gas content determination, the coal samples are exposed so that the escaping gas during the sampling process is hard to quantified, which mainly affects the accuracy of the gas content. To overcome this limitation, some studies have improved the coring process from the coring mechanical devices, such as sealed coring (Long and Sun, 2021), negative pressure pneumatic conveying coring (Wen et al., 2017), compressed air ejector sampling method (Zou and Zhang, 2009), inhibition of gas desorption (low temperature coring) (Wang et al., 2019), and core wrapping with sealing fluid (Qi et al., 2010), and other ideas for gas content parameter determination technology and equipment upgrade. Xie Heping's group proposed the "principle and technology of in-situ pressure and gas-preserved coring in coal mines" and independently developed coring equipment and in-situ gas content measurement device (Gao et al., 2021). This coring equipment has developed a saddle-shaped pressure-holding controller using the geometric principle of Mouhe square cover, adopts multiple anti-rotation coring structures, and realizes low-disturbance downhole in-situ coring. The coring system has the advantages of stronger capacity of pressure holding, lower disturbance, and higher efficiency of the drilling coring than the others (Xie et al., 2023; Gao et al., 2021; Liu et al., 2023; Wang T. et al., 2023; Shi et al., 2023; Zhu et al., 2023; Liang et al., 2023; Cui et al., 2023; Huang et al., 2023a, b).

The precision of gas content analysis is closely linked to the coring method used. Although the technical equipment for in-situ collecting gas-preserving coal samples has made breakthroughs, the determination of in-situ coalbed core parameters is also particularly affected by the drilling depth, because of the excavation damage and drilling disturbance that would cause zoning rupture around the borehole and roadway. The unloading of excavation and drilling at different depths can lead to different degrees of failure and damage (Meng et al., 2013; Yuan et al., 2014; Hungerford and Ren, 2014). Reducing the exposure time of a sample to its environment minimizes the disturbance caused by excavation and drilling, which leads to more accurate results in determining gas

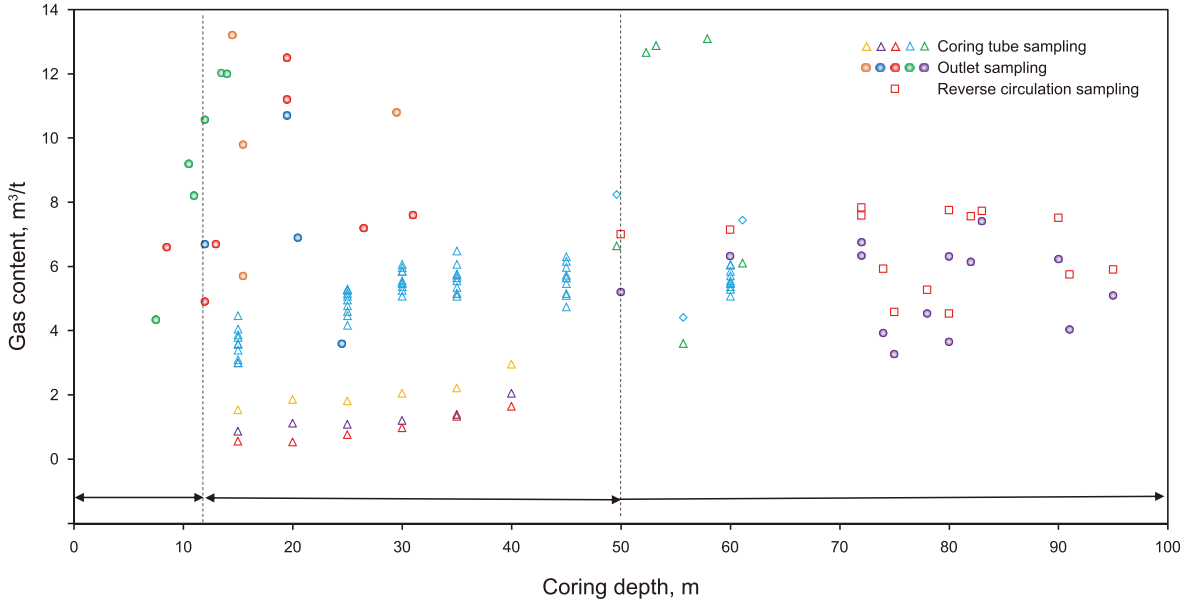

Fig. 1. Coal seam gas content at different coring depths using coring tube sampling, outlet sampling, and reverse circulation sampling.

content, as per engineering practice. Thus, the determination of in-situ coring depth of the coal seam is a prerequisite for obtaining in-situ gas content information.

The excavation of roadways and the disturbance of the coring drilling will inevitably cause large deformation and displacement of the surrounding coal seam. The determination of coring depth in coal seam involves complex physical problems and mechanical behaviors and is a lack of numerical method considering the influence of in-situ geological conditions and actual engineering disturbance. The finite element method (COMSOL) needs to be further improved when simulating such large deformation problems (Zhang C.L. et al., 2021). While FLAC^{3D} uses explicit finite difference formulas to solve geotechnical engineering problems, it can model complex behaviors, such as problems consisting of multiple stages, large displacement and large strain problems, nonlinear material behavior or unstable systems, and even extensive yield/failure or complete collapse. It is challenging to use a single numerical simulation method to fully analyze the coupling of multiple physical fields of gas migration under the influence of large deformation.

Therefore, a multi-physical field of stress distribution and gas migration in coal seam needs to be considered in the coupling model by the combination of FLAC^{3D} and COMSOL Multiphysics to explore the in-situ gas release law under the excavation and drilling disturbance at different coring depths. The simulation data are utilized to investigate the evolution characteristics of the stress field and seepage field in the coal seam. This analysis is done for different coring depths after roadway excavation and drilling disturbance. Additionally, the difference in gas content determined by pressure-preserved coring is compared with the method of traditional drilling cuttings, it provides scientific basis for decision making on drilling depth in-situ pressure-preserved coring in coal seams.

2. Fundamental mechanisms and theories

2.1. Drilling disturbance during coring in coal mine

Due to the formation and evolution characteristics of the excavation disturbed zone in the surrounding rocks, numerous scholars have researched the development of fissures (Harrison et al., 2002), surrounding rock wave velocity and permeability coefficient (Martino and Chandler, 2004), to reveal the zoning characteristics of surrounding rock caused by excavation. At the same time, the effect of stress redistribution, burial depth, and other factors on the disturbance area of roadway excavation was explored through numerical simulation (Zhou et al., 2017). The relevant research on gas migration law in coal seams was usually focused on burial depth (Hao et al., 2017), initial permeability (Zhang C.L. et al., 2021), and different drilling conditions, and relevant gas-solid coupling model. On this basis, the slippage effects (Xiao and Pan, 2005), temperature effects (Liang et al., 1996), adsorption expansion stress (Yin et al., 2008), and other factors are also considered, respectively. However, the process of drilling and coring involves multi-field coupling, and the drilling disturbance is affected by the interaction and joint influence of multiple factors. The 3D gas-solid coupling model can aid in a deeper comprehension of the gas migration pattern (Yin et al., 2013).

The excavation and drilling on the roadway can directly change the stress field, seepage and diffusion field of the coal seam gas surrounding the borehole, which will also show a coupling relationship between them. Therefore, this study first establishes a multi-physics coupling model of gas migration in roadways. The excavation and drilling disturbance of the roadway or borehole can change the original stress equilibrium state until reaching a new equilibrium. As the stress state changes during progress, cracks, and deformation localization form in the surrounding rock at varying degrees of damage. These damage zones then become the preferred channels for gas migration. Coal is a type of material that is composed of two porous mediums, i.e., the coal matrix and the coal fractures. Driven by the concentration gradient, the gas containing in the coal matrix moves to the coal fractures through diffusion. Additionally, the gas in the fracture flows through seepage, which is driven by pressure gradient. The pressure and concentration gradient of the gas drive the conversion of the gas adsorbed in the pores into the free gas, which then migrates into coal fractures. Thus, it is important and beneficial to consider the effects of roadway excavation and drilling disturbance on the distribution of in-situ gas, such that to determine the coring depth to get in-situ coal samples and in-situ gas parameters.

2.2. Mechanical and seepage model

2.2.1. Stress field

The cohesion of coal decreases when new cracks occur due to stress exceeding the yield stress of the coal. The mechanical performance and properties of the coal are described using the strain softening model (Pourhosseini and Shabanimashcool, 2014), as shown in Eq. (1) (the specific definitions of parameters in all equations in this article can be found in Appendix A).

$$c = \begin{cases} c_0 - (c_0 - c_1)\gamma^{\mathrm{p}}/\gamma^{\mathrm{p}^*}, 0 < \gamma^{\mathrm{p}} < \gamma^{\mathrm{p}^*} \\ c_1, \gamma^{\mathrm{p}} \geq \gamma^{\mathrm{p}^*} \end{cases} \tag{1}$$

The incremental softening parameter (γ^p) is determined by the plastic strain increments, as shown in Eq. (2) (Tu et al., 2018).

$$\gamma^{\mathrm{p}} = \sqrt{\frac{2}{3}\left(\varepsilon_1^{\mathrm{p}}\varepsilon_1^{\mathrm{p}} + \varepsilon_2^{\mathrm{p}}\varepsilon_2^{\mathrm{p}} + \varepsilon_3^{\mathrm{p}}\varepsilon_3^{\mathrm{p}}\right)} \tag{2}$$

The plastic strain increments Eq. (3) can be acquired through the utilization of the plastic potential function $g\left(\sigma_{ij}, \gamma^{\mathrm{p}}\right)$:

$$\dot{\varepsilon}_{ij}^{\mathrm{p}} = \delta\frac{\partial g}{\partial \sigma_{ij}} \tag{3}$$

2.2.2. Matrix gas diffusion equation

The Eq. (4) represents the conservation of mass in the flow of gas through coal matrix:

$$\frac{\partial m_{\mathrm{m}}}{\partial t} = -Q_{\mathrm{S}} \tag{4}$$

The value of m_{m} is obtained using the Langmuir equation and the ideal gas state Eq. (5).

$$m_{\mathrm{m}} = \frac{V_{\mathrm{L}}p_{\mathrm{m}}}{p_{\mathrm{m}} + p_{\mathrm{L}}}\cdot\frac{M_{\mathrm{C}}}{V_{\mathrm{M}}}\rho_{\mathrm{C}} + \varphi_{\mathrm{m}}\frac{M_{\mathrm{C}}}{\mathrm{R}T}p_{\mathrm{m}} \tag{5}$$

Q_{S} can be calculated by Eq. (6).

$$Q_{\mathrm{S}} = \frac{1}{\alpha}\frac{M_{\mathrm{C}}}{\mathrm{R}T}\left(p_{\mathrm{m}} - p_{\mathrm{f}}\right) \tag{6}$$

By plugging in Eqs. (5) and (6) into Eq. (4), we can derive the matrix gas diffusion Eq. (7).

$$\frac{\partial p_{\mathrm{m}}}{\partial t} = -\frac{V_{\mathrm{M}}\left(p_{\mathrm{m}} - p_{\mathrm{f}}\right)\left(p_{\mathrm{L}} + p_{\mathrm{m}}\right)^2}{\alpha \mathrm{R}TV_{\mathrm{L}}p_{\mathrm{L}}\rho_{\mathrm{C}} + \tau\varphi_{\mathrm{m}}V_{\mathrm{M}}\left(p_{\mathrm{L}} + p_{\mathrm{m}}\right)^2} \tag{7}$$

2.2.3. Fracture gas seepage equation

The Eq. (8) that represents the conservation of mass for cracked gas is:

$$\frac{\partial m_f}{\partial t} = -\nabla\left(\rho_f v_f\right) + Q_S \tag{8}$$

m_f is expressed as Eq. (9).

$$m_f = \varphi_f \rho_f \tag{9}$$

The state equation of an ideal gas can be used to calculate ρ_f, as shown in Eq. (10).

$$\rho_f = \frac{M_C}{RT} p_f \tag{10}$$

Darcy's law can be used to calculate the value of v_f, as shown in Eq. (11).

$$v_f = -\frac{k}{\mu}\nabla p_f \tag{11}$$

By plugging Eqs. (9)–(11) into Eq. (8), we can derive the Eq. (12) that describes gas flow in fractures.

$$\partial\left(\varphi_f p_f\right)/\partial t = -\nabla\left(\frac{k}{\mu} p_f \nabla p_f\right) + \frac{1}{\tau}\left(p_m - p_f\right) \tag{12}$$

2.2.4. Permeability evolution equation

The relationship between volume strain and permeability is expressed as Eq. (13) (Xie et al., 2013).

$$k_1 = \frac{k_0}{1+\varepsilon_V}\left(1 + \frac{\varepsilon_V}{\varphi_{f0}}\right)^3 \tag{13}$$

The expansion and deformation caused by matrix adsorption have an impact on the evolution of cracks and result in effective stress changes, as shown in Eq. (14).

$$\varphi_f = \varphi_{f0} + \frac{(1+\nu)(1-2\nu)}{E(1-\nu)}\left(\alpha_f p_f + \alpha_m p_m - \alpha_f p_{f0} - \alpha_m p_{m0}\right) - \frac{2(1-2\nu)}{3(1-\nu)}\left(\frac{\varepsilon_L p_m}{p_m + p_L} - \frac{\varepsilon_L p_{m0}}{p_{m0} + p_L}\right) \tag{14}$$

The permeability evolution equation obeys the cubic law, which describes the relationship between the permeability and the porosity of the coal, as shown in Eqs. (15) and (16)

$$k = k_0\left(\frac{\varphi_f}{\varphi_{f0}}\right)^3 \tag{15}$$

$$k = k_1\left\{1 + \frac{(1-2\nu)}{\varphi_{f0}(1-\nu)}\left[\frac{(1+\nu)}{E}\left(\alpha_f p_f + \alpha_m p_m - \alpha_f p_{f0} - \alpha_m p_{m0}\right) - \frac{2\varepsilon_L}{3}\left(\frac{p_m}{p_m + p_L} - \frac{p_{m0}}{p_{m0} + p_L}\right)\right]\right\}^3 \tag{16}$$

3. Simulation scheme

3.1. Simulation workflow

During roadway excavation and drilling, the coal seam undergoes unloading and thus, its stress is rebalanced. This can lead to significant displacement and deformation of the coal body, as it is subjected to the in-situ stress. However, the COMSOL has poor convergence when dealing with large deformation and large displacement, especially when the 3D simulation is carried out in rock mechanics. To further utilize the advantages of the COMSOL in multi-physical field coupling and fluid flow, and avoid its limitation in simulating large deformation and large displacement, this paper adopts finite difference software FLAC^{3D} to simulate large displacement and large deformation in coal seam excavation and drilling process. In this study, the FLAC^{3D} is innovatively used to simulate the roadway excavation and borehole drilling, and a code was written to import volume strain data as raw data into COMSOL. This code was used to investigate gas diffusion and seepage laws while taking into account the influence of roadway excavation and various drilling depths.

Firstly, a FLAC^{3D} model was established based on the physical mechanics and geological parameters of the in-situ stratum of the coal seam. Tunnel excavation and drilling conditions were imposed based on the in-situ stress state of the coal seam, and finally the coal seam body deformation based on FLAC^{3D} was obtained. The numeric model with the same geometric dimensions and parameters was established by COMSOL and FLAC^{3D} software. The volume strain data of the coal seam was imported into the COMSOL using interpolation. Based on the relationship between volume strain and permeability, the calculation results formed by tunnel excavation and borehole drilling were used as the basic parameters for COMSOL to simulate gas migration, and a numerical simulation study was conducted considering the influence of tunnel excavation and borehole drilling disturbances. It can fully take the advantages of FLAC^{3D} in simulating large deformation engineering and COMSOL in simulating multi-physics fluids migration. The study finally verified the reliability of calculation results through on-site monitoring data (Xue et al., 2017; Luo et al., 2010).

Fig. 2 displays the use of FLAC^{3D} to create a geometric model that aligns with the lithologic distribution of the formation. Boundary conditions and initial values are provided to quantify the evolution of the stress field as the tunnel is excavated at various drilling depths. The strains were exported and imported into COMSOL using a self-written code set. The study builds a geometric model consistent with FLAC^{3D} in COMSOL, and discusses the exploration of the gas migration law during roadway excavation and drilling at varying depths. This exploration was done by determining the initial permeability of the area through volume strain and permeability relationship. The Darcy seepage field and partial differential equation module were then utilized to study fracture seepage and matrix diffusion while considering the heterogeneous initial permeability distribution.

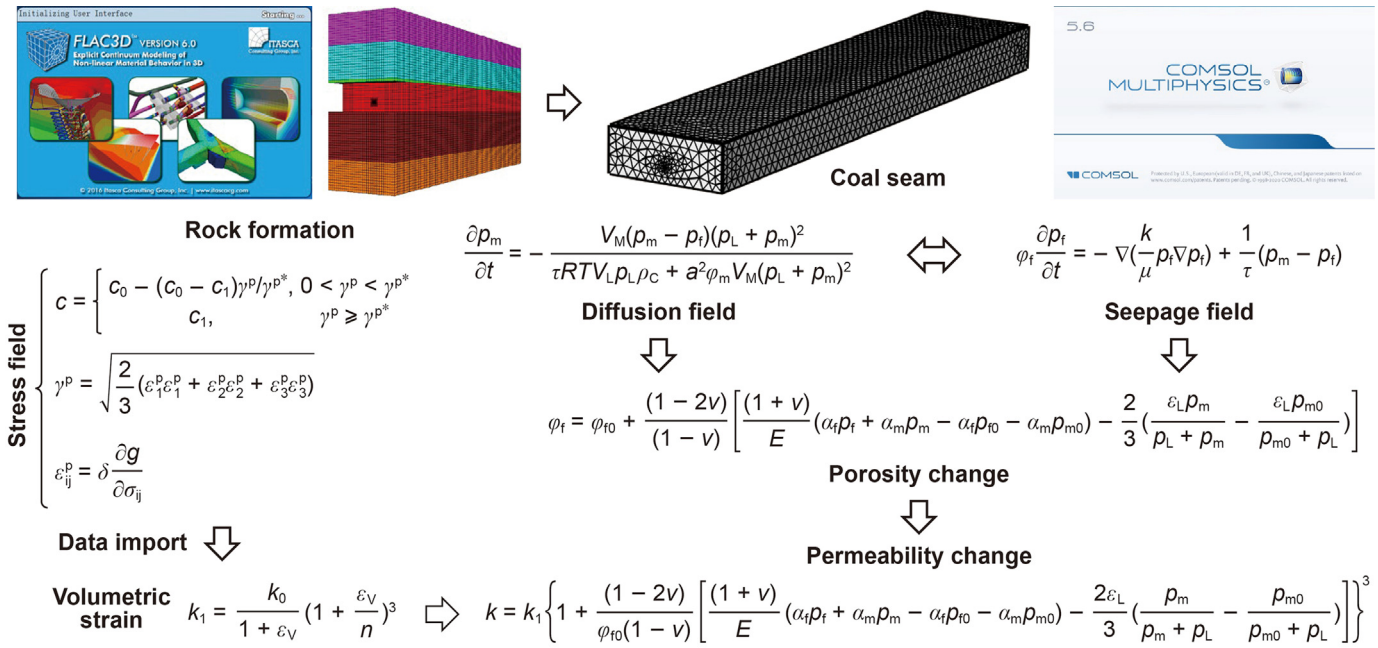

Fig. 2. Simulation scheme and workflow of coupling stimulation by COMSOL and FLAC^{3D}.

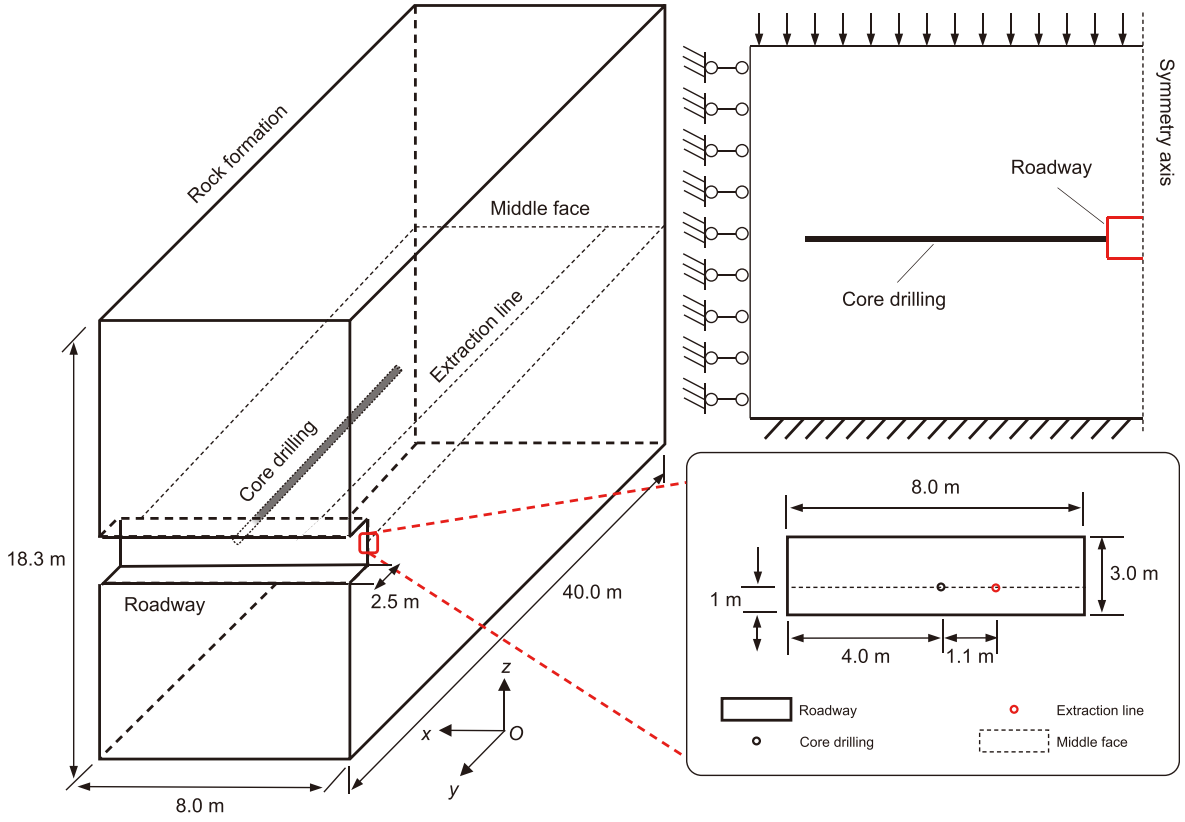

Fig. 3. Geometric model and engineering background of roadway excavation and coring drilling in the coal seam.

3.2. Geometric model and boundary conditions

The in-situ gas content determination results typically rely on the coal seam conditions, which are influenced by gas desorption and migration that are sensitive to mining and excavation. Therefore, in this study, the modeling of the geological conditions of the roadway in the undisturbed zone of the working face is utilized (Gao et al., 2012, 2020). Fig. 3 displays a cubic geometric model with a size of 8.0 m × 40.0 m × 18.3 m. The model includes a roadway in the middle with a size of 3.0 m × 8.00 m × 2.5 m. The

Table 1
Grid parameters, basic physical and mechanical parameters used for numerical simulation.

Parameters	Value	Parameters	Value
Coal seam temperature, T	305.15 K	Methane dynamic viscosity	1.08E-5 Pa•s
Limit adsorption deformation of coal	0.004	Adsorption time	0.5 d
Initial porosity of fractures, φ_f	0.018	Langmuir volume constant, V_L	21.44 m^3/t
Initial matrix porosity of coal, φ_m	0.0532	Density of coal, ρ	1290 kg/m^3
Initial permeability of coal, k_0	1.445×10^{-17} m^2	Initial gas pressure of coal seam, p_0	6E5 Pa
Poisson's ratio of coal, ν	0.3	Langmuir pressure constant, p_L	8.7E5 Pa
Max size of the unit	0.194	Min size of the unit	0.021
Growth rate of the max unit	1.1	Curvature factor	0.4
Narrow area resolution	0.9	Ideal gas constant	8.41351 J/mol/K

roadway contains a Φ114 mm coring borehole positioned at 1.0 m away from the roadway floor. Additionally, a parallel cut is made to the middle face at a height of 1.0 m from the floor of the roadway, and an extraction line is set on the middle face at a distance of 1.1 m along the *X*-axis from the coring hole. Grid parameters setting in the numerical simulation can be found in Table 1.

This schematic in Fig. 3 displays the model's boundary on the *YZ* plane. The rock layer's bottom is a fixed boundary, and a vertical stress of 16 MPa (~700 m) is applied at the top (in the study, the 16 MPa stress was applied by surface force. And a stress gradient of 0.022e6 along the *Z* direction is applied. The stress is calculated by considering the self-weight of the overlying rock layer and the burial depth ($\sigma v = \rho g h \approx 2286$ kg/m^3 $\times$ 10 N/kg $\times$ 700 m $\approx$ 16 MPa). The left, right, front, and back sides are all rollers boundary. As for the coal seam boundaries, both the top and bottom boundaries are zero flux in the COMSOL Multiphysics. In the simulation process, the roadway is excavated first, and then the core drilling is carried out. Table 1 (Wang et al., 2023; Liu et al., 2020) and Table 2 (Yao, 2022) present the mechanical parameters and model diagrams for each rock layer during the simulation process. FLAC^{3D} was employed to conduct simulations based on the original size and geological information of the roadway to investigate the impact of in-situ gas migration caused by excavation disturbance of the roadway and drilling. The volume strain of the plastic zone formed by tunnel excavation and borehole drilling was extracted and then inputted into COMSOL for the purpose of calculating permeability and simulating gas seepage. To summarize, the study utilized FLAC^{3D} for simulation, and then imported the extracted volume strain data into COMSOL for permeability calculation and gas seepage simulation. The basic assumptions of this numerical simulation are that: a) The coal is a dual medium of pores and fissures; b) The adsorbed gas molecules in the pores desorb from the surface of the coal particles and become free; c) The free gas diffuses into cracks through pores, and its diffusion pattern conforms to Fick's diffusion law; d) The free gas seepage in the cracks flows into the borehole or tunnel, and its flow pattern complies with Darcy's law.

4. Results

4.1. Vertical stress around borehole under different coring depths

The geological conditions of the coring location, coring process, and coring depth affect the in-situ gas content and gas pressure. Previous lab studies and simulations have determined that the excavation disturbed zone in the coal seam extends up to ~8 m away from the wall of the roadway to the monitoring point. Therefore, simulation coring depths were selected as 5, 8, 9–15, 20, 25, and 30 m. Fig. 4 shows that for coring depths less than 20 m, the stress-affected zone of the borehole gradually extends with increasing coring depth. However, the vertical stress-affected stage of roadway excavation does not change significantly. For coring depths of 25 and 30 m, the influence range of vertical stress gradually extends round surface to the bottom of the borehole. The vertical stress during the excavation stage firstly increases and then decreases from the roadway wall along the drilling direction, with the vertical stress peak reached at approximately 9 m. At different coring depths, clustered stress concentration areas are present at 9–12 m away from the roadway wall. These areas may result from the superposition of the stress concentration zones created by the roadway excavation and drilling disturbance.

To quantitatively analyze the distribution characteristics of vertical stress, data in the extraction line at different coring depths were extracted for analysis. Fig. 5 shows that the vertical stress around the borehole at different depths exhibits a pattern of initially increasing to a peak value and then gradually decreasing to a certain stress value as the distance from the road wall increases. The stress distribution at different coring depths can be divided into three sections from the roadway wall to a drilling depth of 40 m.

The first section, called the stress reduction zone or stage A, extends from the roadway wall to about 5.5 m away from it. As excavation progresses, the stress in this section is unloaded into a stress relief zone, causing the overall stress in this section to be lower than that of the original rock.

Table 2
Geological and mechanical information of different rock formations.

Lithology	Thickness, m	Cohesion, MPa	Friction	Tensile strength, MPa	Bulk modulus, GPa	Shear modulus, GPa	Constitutive model
Fine sandstone	3.21	10.20	38.60	2.85	9.10	5.90	Mohr-Coulomb
Sandy mudstone	3.62	8.22	38.60	2.85	5.20	3.10	Mohr-Coulomb
Mudstone1	0.28	6.80	38.30	1.00	2.40	1.10	Mohr-Coulomb
Coal	3.02	1.40	31.00	0.72	1.30	0.60	Strain Softening
Mudstone2	4.98	6.80	35.60	2.00	7.20	4.00	Mohr-Coulomb
Siltstone	3.22	6.80	35.60	2.00	13.30	9.20	Mohr-Coulomb
Roadway	/	1.40	31.00	0.72	1.30	0.60	Strain Softening
Borehole	/	1.40	31.00	0.72	1.30	0.60	Strain Softening

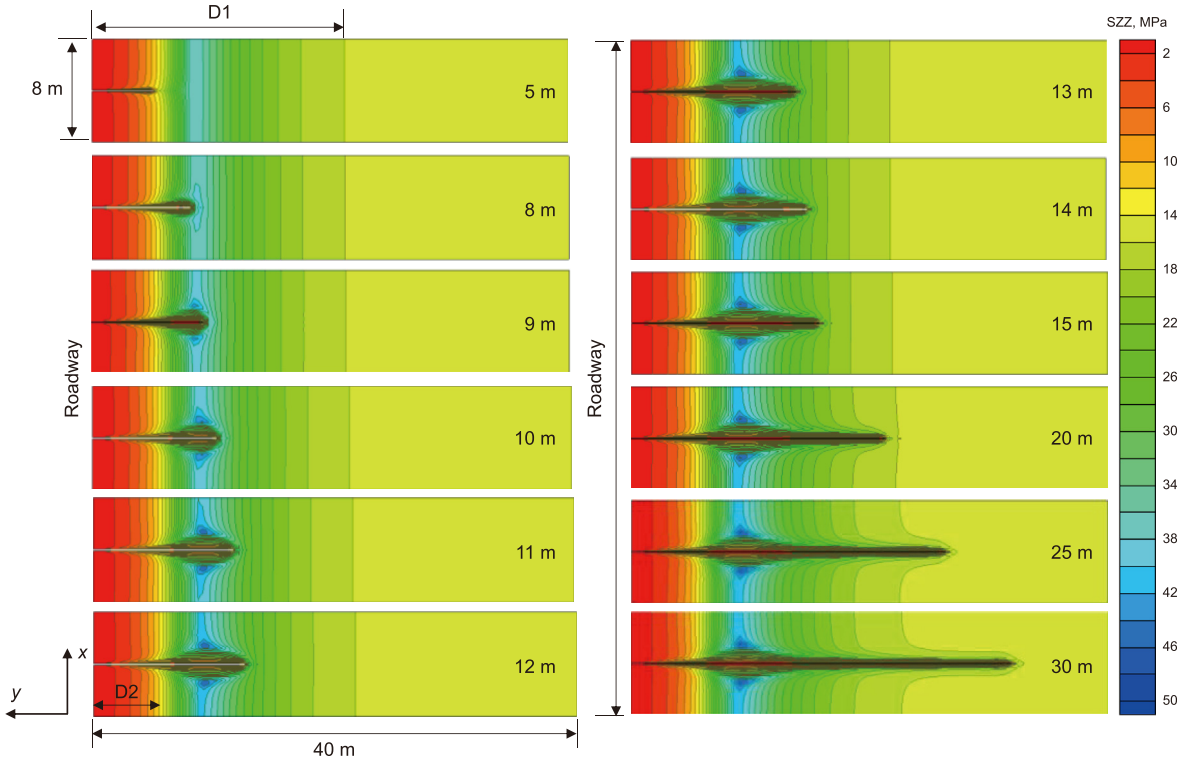

Fig. 4. Cloud map of vertical stress distribution of coal seam under different coring depths.
(D1 is the vertical stress-affected stage of roadway excavation, and D2 is the core drilling depth; The stress state in the coal seam under different drilling depths shows negative values in the simulation results and software, which means that the overall stress on the coal seam is compressive stress. To facilitate comparison of stress magnitudes, the stress gradient in the cloud diagram here is set to a positive value.)

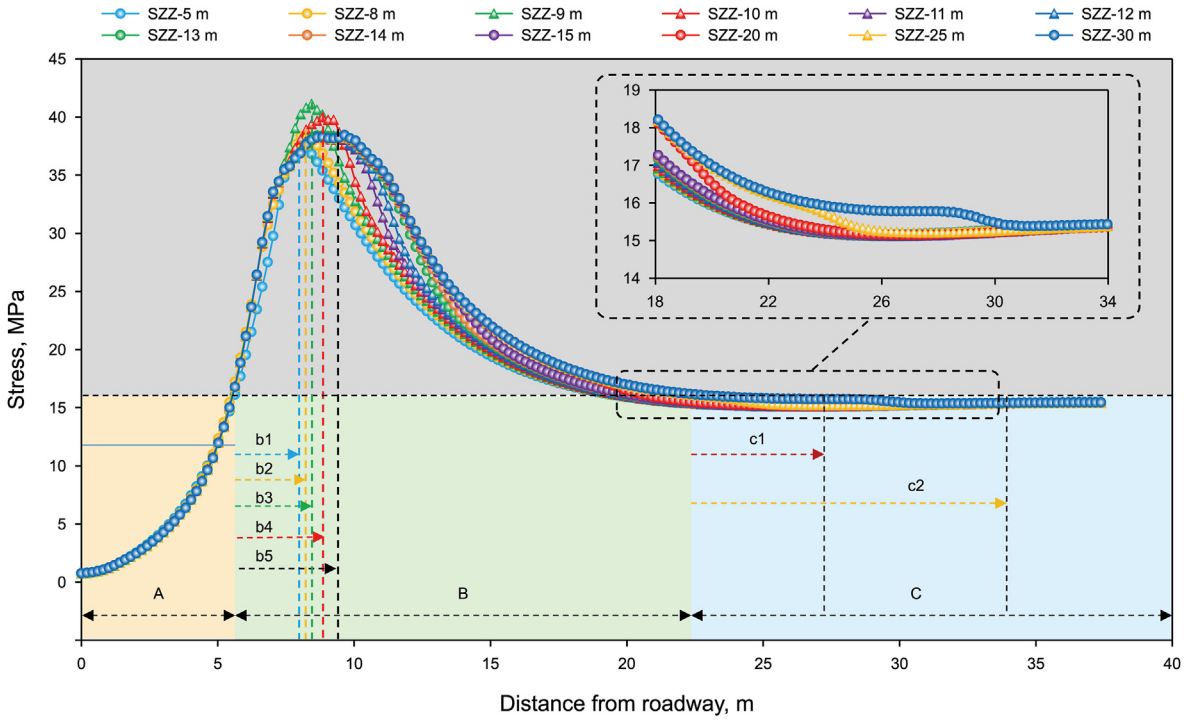

Fig. 5. Vertical stress distribution curves at different coring depths in coal seam.

The second section, called the stress increase zone or stage B, extends from 5.5 to 22 m away from the wall of the roadway. The stress in this section first increases to a peak value and then gradually decreases to the original rock stress. When the coring

depth is < 11 m, the peak stress increases gradually with drilling depth, and the distance away from the wall of the roadway at the peak stress also increases. After reaching a depth of 11 m, the peak stress, and its corresponding distance from the initial boundary of the stress rise zone do not change significantly.

The third section is the original rock stress zone or stage C, which extends from 22 to 37.55 m away from the roadway wall. The stress in this section is less affected by roadway excavation and gradually tends to the original stress. The distance from the tunnel wall corresponding to the vertical stress decreases to the original stress gradually delayed with the increase of the coring depth.

Based on the stress distribution at different coring depths, the surrounding rocks of the drilling borehole can be divided into stress relief zone, stress concentration zone, and original rock stress zone. The stress concentration zone should be further subdivided into the elastic zone, high-stress concentration zone, and stress recovery zone.

4.2. Permeability around borehole under different coring depths

The permeability slice depicted in Fig. 6, indicates a distinct partition phenomenon in the permeability of the surrounding rocks of the roadway when extracted along the middle face. The permeability distribution is symmetrically distributed along the borehole. From roadway wall to drilling depth, it can be roughly divided into four different areas, as shown in the stage E1 of Fig. 6, the permeability of this stage is higher than other stages, and the permeability gradually decreases from roadway wall to drilling depth; the permeability of stage E2 is lower than that of stage E1, and the permeability gradually decreased along the drilling direction of the borehole; extending to the depth of the borehole is the stage E3, this stage only has a high permeability value around the borehole, and the other parts have low permeability values. The coal seam permeability minimum value is broadly dispersed in this area, and the E4 stage extends deeper into the borehole, and the permeability distribution around the borehole in this stage has obvious changes, and the permeability of the stage closest to the borehole is higher.

The further away from the central axis of the borehole, the lower the permeability, and a stage is reached where the permeability is at its minimum. The permeability of other parts of this stage is uniformly distributed; the final stage extending into the borehole is E5, and the permeability of this stage is uniformly distributed. The radial direction of the borehole is significantly affected by drilling disturbance, whereas its axial direction is minimally impacted. Taking a stage through the center of the borehole perpendicular to the middle face, the permeability of the coal seam surrounding the roadway exhibits variation at different coring depths. It has been observed that as the coring depth increases, the permeability also changes. The permeability in the E1 and E3 stages remains relatively consistent, but the E3 stage shows different permeability distributions at coring depths of 5, 8, and 9 m. Beyond a coring

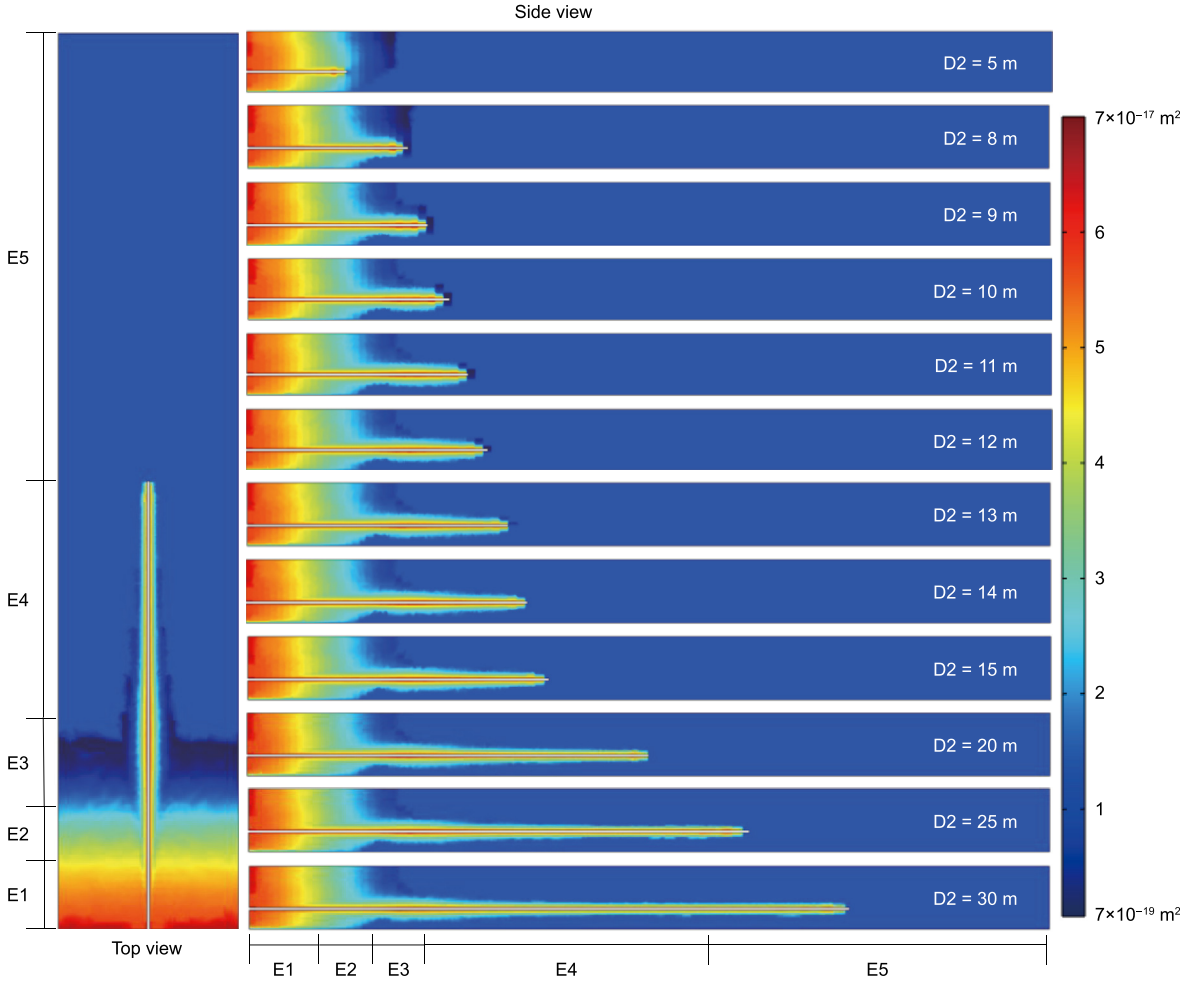

Fig. 6. Cloud map of permeability distribution around borehole at different coring depths in coal seam.

depth of 11 m, the E3 stage does not exhibit any significant changes in permeability distribution. The E4 stage exhibits varying permeability distributions with coring depth, while the permeability of the E5 stage remains unaffected by coring depth.

The permeability distribution in the E1 and E2 stages is primarily impacted by roadway excavation and stress relief. Excavation of the roadway eliminates displacement constraints, causing coal mass to unload into the roadway and resulting in high permeability in this stage. The E3 stage is a stress concentration area, and the coal body in this stage undergoes further compression due to high in-situ stress, leading to a significant decrease in permeability. The stress in the E4 stage is further reduced, and its distribution is influenced by roadway excavation, causing the permeability distribution of this stage to be affected by drilling around the hole. The E5 stage, being the original rock stress area, is not affected by roadway excavation or drilling and remains in its original state, with permeability being evenly distributed.

In the actual calculation process, different permeability models should be defined considering the damage stage for the permeability at different damage stages. However, the permeability model division of different damage stages through COMSOL in this article means that the permeability needs to be divided into different areas, which will further affect the difference in calculation results at different coring depths (if the permeability models of different damage stages are divided into different areas through COMSOL in this article, model division means that the permeability needs to be divided into different areas, which may have a direct impact on gas migration at different coring depths that is the focus of this study). Therefore, in the process of deriving volume strain from the FLAC^{3D} model, this article directly reflects the difference in permeability in different damage stages through the numerical differences in volume strain in different damage areas. A more systematic study of permeability models at different damage stages can be conducted in future research.

4.3. Evolution of gas pressure around boreholes

As the original stress equilibrium state is disrupted, the unloading disturbance of roadway excavation and borehole drilling further lead to a considerable number of cracks inside the coal seam. As cracks form, the adsorbed gas can convert into free coal seam gas, and the free coal seam gas is prone to migrate through the cracks and into the roadway. Additionally, the adsorbed gas in the coal seam transforms into free gas. This process has a direct impact on the gas occurrence law in situ. Therefore, it is necessary to examine the evolution of gas pressure around the borehole. To accomplish this, gas pressure is measured at different times along the extraction line at a coring depth of 20 m. Furthermore, a perpendicular stage is taken at distances of 5, 9, 10, 15, and 20 m from the roadway wall to investigate the distribution of gas pressure perpendicular to the drilling direction.

According to Fig. 7(a), gas pressure around the drilling hole decreases over time, but the trend varies at different depths. As core time passes, gas pressure decreases noticeably from the roadway wall to 5.5 m away, and the pressure distribution increases from the roadway wall to the borehole's depth. From 5.5 to 12 m away, gas pressure around the borehole decreases with core time, but the pressure distribution curve oscillates, fluctuating along the drilling direction. From 12 to 22.5 m away, gas pressure around the roadway decreases with coring time, remaining constant within 22.5 m from the roadway to the borehole's depth for a month. Fig. 7(b)–(f) show that gas pressure around the borehole gradually decreases with time at locations 5, 9, 10, 15, and 20 m away from the borehole wall. Comparing the decline of gas pressure by 0.1 MPa as the evolution criterion reveals that the influence range of unit time is largest at 5 m from the roadway wall, followed by 15, 8, and 9 m, and smallest at 20 m. Permeability distribution in Fig. 6 shows that gas pressure attenuation is significant in the stress relief area around 5 m from the roadway wall. The coal seam at 9 and 10 m is in a state of stress concentration with low permeability and weak gas pressure attenuation. The coal seam at 15 and 20 m is gradually weakened by roadway excavation. The gas pressure attenuation is also weak, which also indicates that it is closer to the in-situ gas pressure occurrence area.

5. Discussion

5.1. Distribution of excavation disturbed zone in coring borehole

It is possible to trace the history of the surrounding coal failure process through the distribution of the excavation damage zone. Therefore, exploring the distribution characteristics of cracks on both sides of the roadway with a borehole peep instrument can reveal the stress distribution law of surrounding rock. The previous study conducted drilling and inspected the fissures in the surrounding rock on both sides of the roadway (Yan, 2021), as shown in Fig. 8, qualitative and semi-quantitative peephole information was obtained both from the left and right sides of the roadway. Since the results indicated that the shape of the roadway has little effect on the damage form of the roadway (Jiang et al., 2005), it is considered that the geological conditions in the literature are consistent with the scope of the typical mine roadway excavation disturbance area in this study. Based on Fig. 8(a), the left side of the roadway can be classified into three different types of drilling zones according to the density of cracks. Zone I is located 0–5.3 m away from the roadway wall. Cracks are developed in the inner wall of this type of area. Zone II is at 5.3–7.6 m of the roadway wall, and there is no obvious distribution of cracks in the inner wall of this type of area. Zone III is located at 7.6–8.6 m of the roadway wall.

In this type of area, there is no fracture distribution on the inner wall of the drilling borehole, but cracks are distributed at some locations. Similarly, In Fig. 8(b), clear partitions can be observed in the drilling borehole located on the right side of the roadway. The distribution patterns of fractures in the partitions of the 2# drilling are in agreement with those found in the 1# drilling. However, in the 2# drilling, zone I is from the roadway wall to 5.1 m, and zone II is from 5.1 to 7.1 m. Zone III is 7.1–8.9 m. These three types of zones are consistent with the zones in Fig. 8(a). Zone E1 corresponds to area I, that is, the stress relief zone is formed in the roadway wall due to stress relief after roadway excavation, and fractures develop in this area. Zone E2 corresponds to zone II. In this region, the road encircling the rock is presently in its elastic phase. The stress of the surrounding rock is greater than the initial rock stress, although it has not yet reached the strength limit of the surrounding rock. Therefore, there is no obvious fracture distribution in this area. Zone E3 corresponds to zone III. The surrounding rock in this region is under the action of in-situ high stress. The rock in the area is situated within a stress concentration zone, but its surrounding fractures are not solely due to vertical stress. Consequently, there are fissures in various locations.

The distribution of fractures in the borehole is a direct reflection of the stress of the distribution of fractures around the coal body, which will certainly affect the distribution of in-situ gas in coal seam. There are many fractures in the borehole in zone I, which provide channels for gas migration. Due to the concentration gradient and gas pressure, significant amounts of gas will be released and alter the gas distribution pattern in situ. The volume of coal in zone II and III is compressed under the influence of surrounding rock stress, and extensive gas migration channels are closed. The in-situ gas distribution state of coal around the borehole

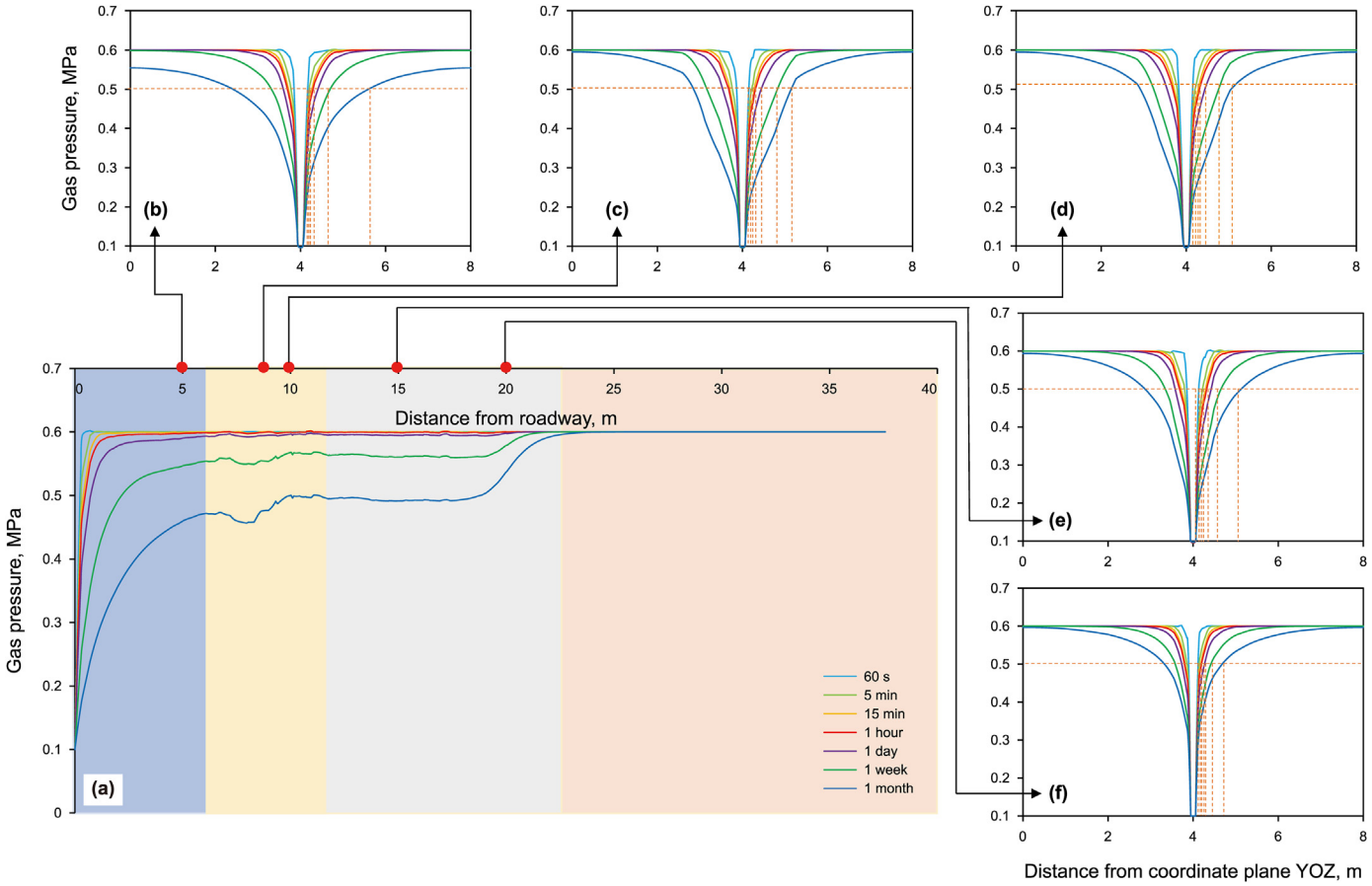

Fig. 7. Gas pressure distribution around borehole under different coring time in coal seam.

at this core-taking depth is also affected by disturbance. The distribution law of coal gas under different core depths will be discussed in the following chapters.

5.2. Distribution of in-situ gas content influenced by roadway excavation time

The distribution of in-situ gas is affected by both roadway excavation and the disturbance of the borehole plastic zone, but the roadway excavation time will also directly affect the in-situ gas distribution characteristics (Zhao et al., 2020). The excavation of the roadway has resulted in extensive cracks in the stress relief zone, providing a high-quality channel for gas migration. However, the coal seam of the stress concentration zone is compressed, forming a "barrier" for gas migration with lower permeability than the original coal seam. The coupling effects of the two sides of the roadway on the original gas pressure distribution deserves further exploration. And it is also an essential influencing factor for the depth exploration of pressure-maintained gas coring. Therefore, numerical simulation only considering roadway excavation without drilling is carried out, and the distribution characteristics of roadway formation time to original gas is explored. The gas content distribution characteristics at different times along the extraction line were extracted.

As demonstrated in Fig. 9, the sequential gas content in the roadway generally decreased within 1.6 m from the roadway wall as the formation time increased. The gas content of the coal seam remained relatively constant. The gas content presents obvious divisions along the roadway wall to the depth beside the roadway. This is shown in F stage, where the divisions are observed from the roadway wall to 5.5 m away from it. Moreover, these divisions increase with the formation time of the roadway. Gas content decrease rapidly at first and then slowly; from the roadway wall 5.5–7 m, as shown in G stage, as roadway formation time increases, gas content decreases rapidly at first and then gradually decreases. However, the rate of change in gas content per unit time is lower than that of stage F; from the roadway wall 7–9 m, as shown in H stage, with the increase of roadway formation time, gas content decreases rapidly at first and then slowly. While the gas content gradually decreases from 9 to 17 m from the roadway wall, the rate of change per unit time is even lower than that of stage H. During the same time of roadway formation, from the roadway wall to the depth, the gas content decay is "exponential" overall. The gas content in F stage drops quickly due to abnormal permeability in the stress relief zone, while that in G stage declines slowly because of stress concentration zone. Therefore, the duration of roadway formation determines the gas content at various depths along the coal seam of the roadway wall. Specifically, if the formation time is one year, the coring depth needs to be at least 17 m.

5.3. Coal seam gas content influenced by coring technique and coring depths

The determination of gas content is influenced by various factors, including differences in core technology that directly affect gas content values. Specifically, varying coring techniques result in different amounts of gas loss; secondly, different coring technique will also directly lead to the different disturbance of excavation and

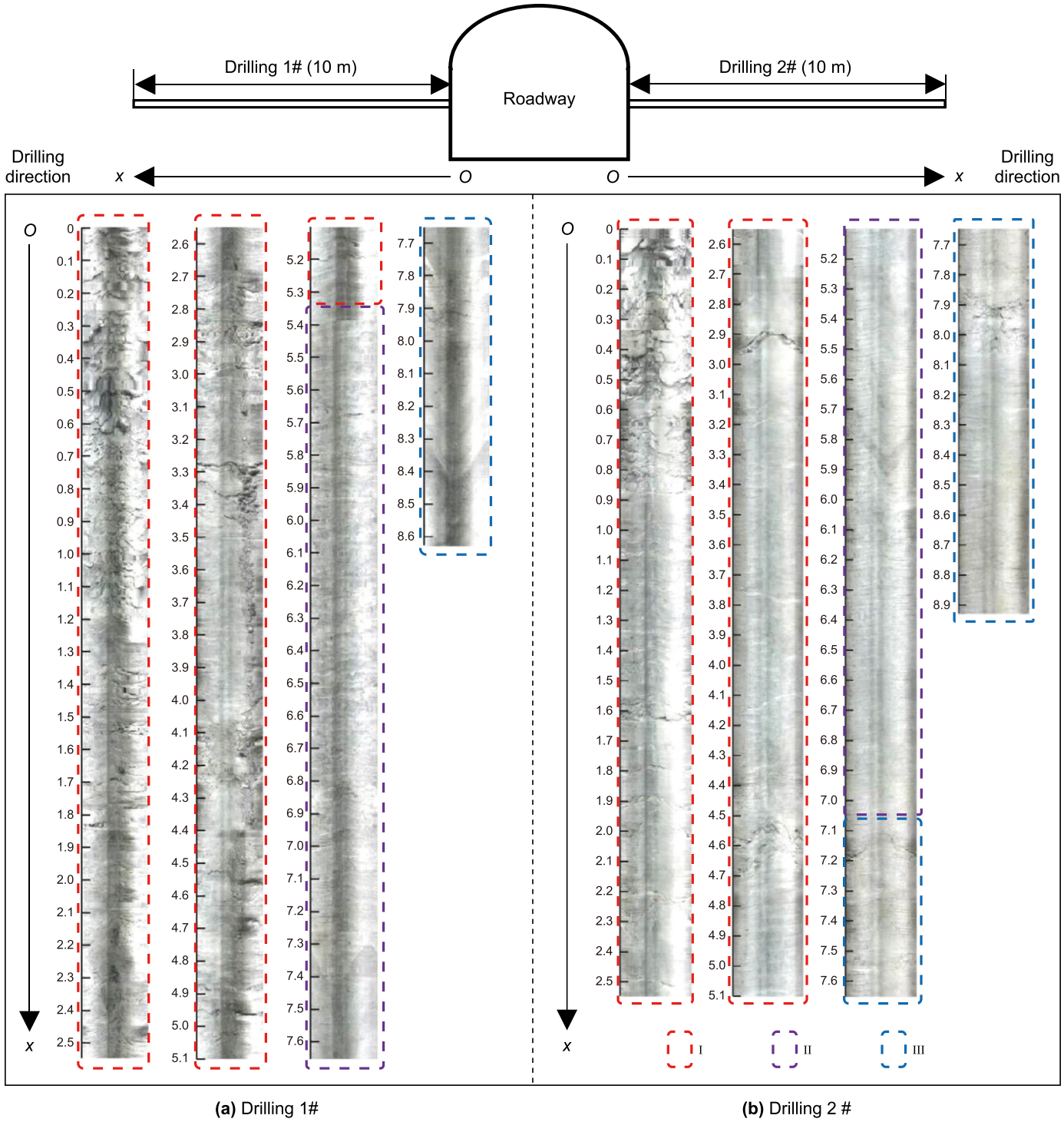

Fig. 8. Identification of excavation damage zone based on the drill peep of boreholes in the side wall of roadway.

drilling on the core, and cause different particle sizes of coal samples, which will directly affect the measurement of gas content. Meanwhile, the difference of measurement methods will also affect gas content, which may lead to the exposure of coal samples in the process of sample transfer, resulting in measurement errors. In the reference the DGC of Chongqing Coal Research Institute was applied to carry out the field determination of gas content at different coring depths (Wei et al., 2019). The gas content (W) under this determination method consists of four parameters:

$$W = W_1 + W_2 + W_3 + W_c \quad (17)$$

$$W_2 = W_{21} + W_{22} \quad (18)$$

$$\text{Amount available for desorption} = W_1 + W_2 + W_3 \quad (19)$$

where W_1 is loss of gas content in coal seam, W_2 is natural desorption gas content before the comminution, W_3 is natural desorption gas content during the comminution, W_c is un-

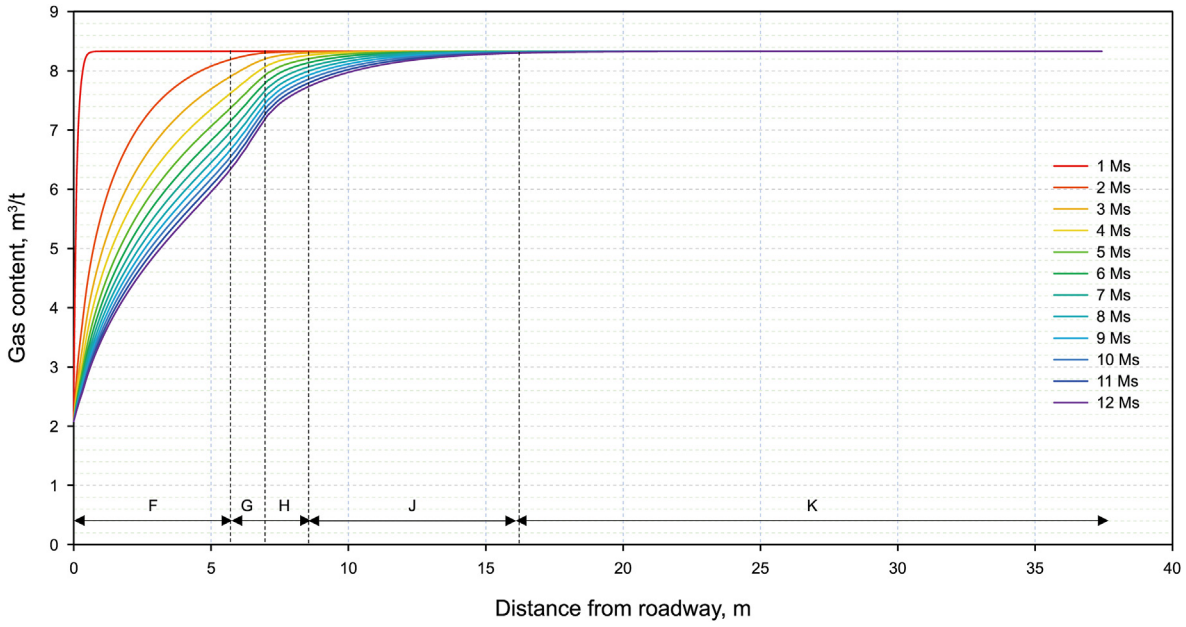

Fig. 9. Time (month) of roadway formation and distribution characteristics of sequential gas content in the coal seam.

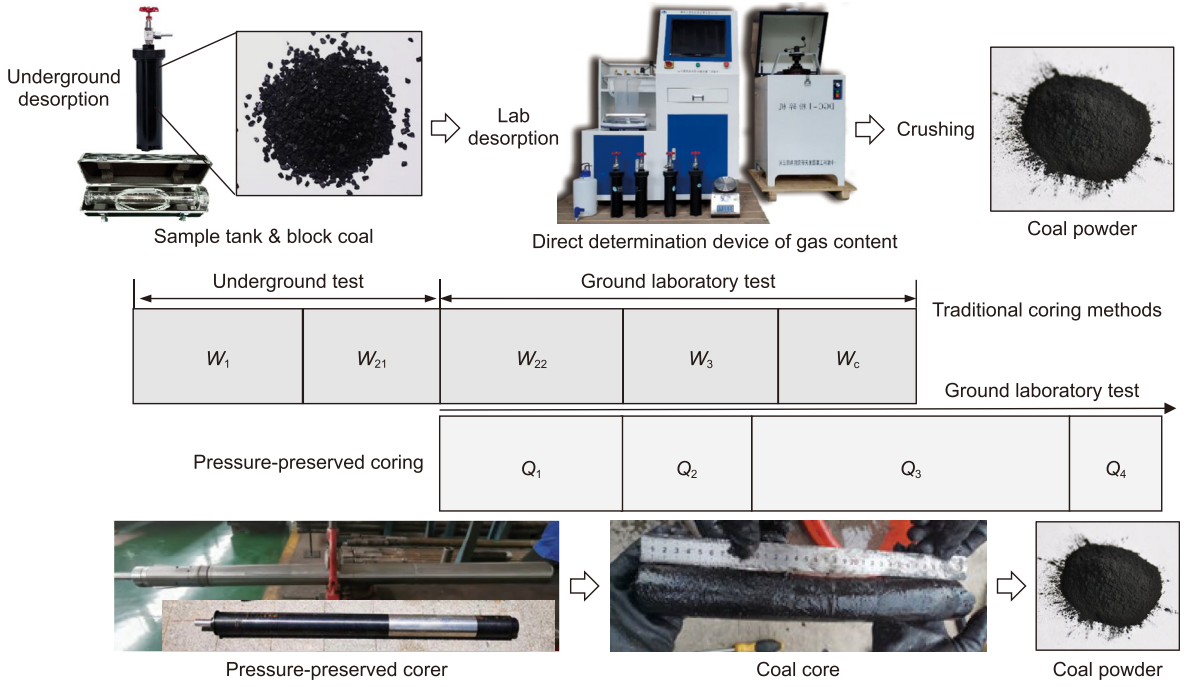

Fig. 10. Comparison diagram of gas content determination by traditional coring methods and pressure-preserved coring.

desorption gas content in normal atmosphere. The coalbed methane content (W) is determined by comprehensively considering four parameters. Among them, the natural desorption gas amount of the pre-crushed coal sample (W_2) includes the underground desorption gas amount (W_{21}) and the surface desorption gas amount (W_{22}). In addition, the CBM content available for desorption includes the gas loss of coal samples (W_1), the natural desorbed gas volume of pre-crushed coal samples (W_2), and the desorbed gas volume of crushed coal samples (W_3).

For the direct determination device of gas content (DGC) gas content determination method, as depicted in Fig. 10, W_1 and W_{21} data need to be measured underground, W_{22} and W_3 are directly measured by laboratory gas drainage device, to obtain the value of W_c, laboratory testing is required to determine basic parameters such as industrial analysis, adsorption constants, porosity, true density, and apparent density of coal samples. For the in-situ pressure-preserved coring in coal seams, the coring operation is carried out under the coal mine, and the determination of the gas content is carried out in the laboratory. The determination of the gas content of the pressure-preserved coring test consists of four parts. The first part of gas content Q_1 is primary desorption gas, the second part of gas content Q_2 is transferred desorption gas, the

Table 3
Gas content of coring depths and sampling by pressure-preserved coring and traditional coring.

Coring No.	Coring depth, m	Pressure-preserved coring, m^3/t	Traditional coring, m^3/t	Difference	Coring site
1	5	0.64	0.42	0.52	North Shaanxi
2	6	1.33	0.53	1.51	North Shaanxi
3	6.5	1.53	0.77	0.99	North Shaanxi
4	9	1.55	0.83	0.87	North Shaanxi
5	15	2.04	0.65	2.14	North Shaanxi
6	38	3.72	2.46	0.51	Northeast
7	42	3.57	2.51	0.42	Northeast
8	50	5.19	3.72	0.39	Northeast
9	60	4.69	3.47	0.35	Northeast

third part of gas content Q_3 is pulverizing desorption gas, and the fourth part of gas content Q_4 is un-desorption gas content in normal atmosphere. The gas content measured by the pressure-maintained gas cored satisfies $Q = Q_1 + Q_2 + Q_3 + Q_4$. The gas contents obtained from different coring methods at the different coring depths show in Table 3.

The in-situ pressure-preserved coring process has four advantages compared to the traditional method. Firstly, the coal sample is sealed in the corer at the depth of the borehole. And there is no need to collect loss amount of coal seam gas to calculate W_1 when the coring time was extremely short and on-site loss of gas was minimal, thus, the W_1 could be neglected as the free gas is trapped during in-situ corer closed and pressure preserving, which effectively enhance the determination accuracy of gas content and avoids estimation errors of loss of coal seam gas. Secondly, compared with the traditional drilling cuttings coring method, the coal sample obtained by the in-situ pressure-preserved coring (slightly disturbed coring with multiple anti-rotation) has better integrity of the coal core, avoiding the exposure of more surface area of the coal sample, which is conducive to more accurate determination of adsorbed gas content; thirdly, the coring process has a matching content determination device, which can realize the airtight transfer of coal samples, effectively avoid the gas escape during the sample transfer process, and then the error of gas content determination is avoided; fourthly, the process efficiency of gas content determination can be improved, resulting in more

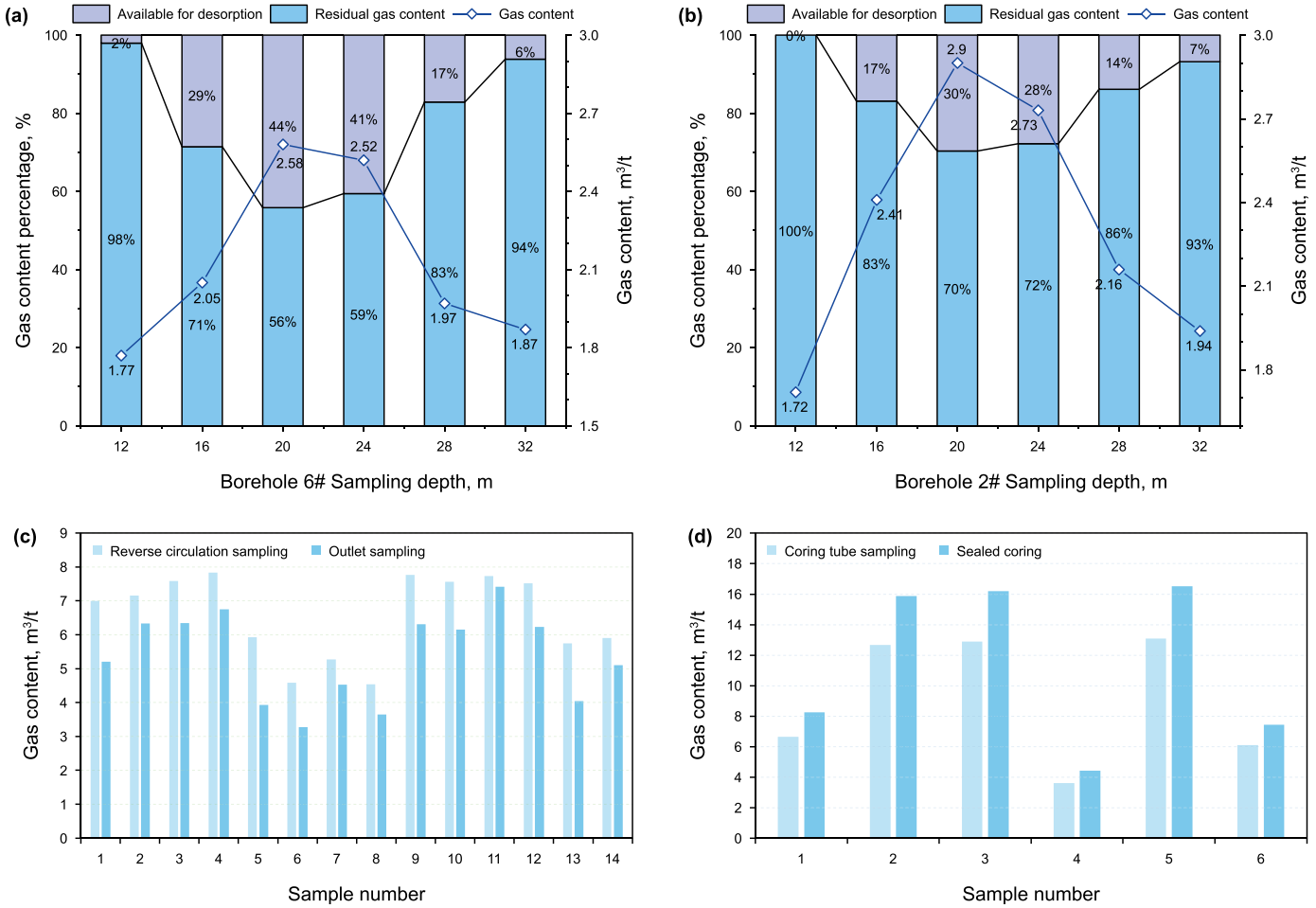

Fig. 11. Measured value and composition percentage of gas content under different coring techniques at different drilling coring depths: (**a**) borehole 6# with outlet sampling; (**b**) borehole 2# with outlet sampling; (**c**) comparation of reverse circulation sampling and outlet sampling; (**d**) comparation of coring tube sampling and sealed coring.

accurate results obtained in a shorter time.

Taking the traditional drilling cuttings coring method as an example, the literature carried out on-site measurement of gas content at different coring depths (Wei et al., 2019), as shown in Fig. 11(a) and (b). It is buried at a depth of about 600 m. The geological conditions are comparable to the typical mine simulation parameters in this study. Consistently, the gas content determination of 13 kinds of coring depths was carried out for 12 boreholes on site. As shown in Fig. 11(a) and (b), in the same borehole, when the coring depth increases, the gas content first increases and then decreases, and the maximum value of gas content is between 20 and 24 m. The on-site gas content measurement data is consistent with the simulated data, which further verifies the reliability of the model in this study. At the same time, when the coring depth is greater than 20–24 m, as the coring depth increases, the time between completing the coring and the coal sample entering the sample tank also increases, which increases the exposure time of the coal sample and further leads to gas escape, thus, the gas content is further reduced. Fortunately, the pressure-preserved coring process can effectively avoid these effects. The coal sample is sealed in the coring device as a unit, so the gas content of the sample should not be affected by the depth of coring, comparing with the coring techniques such as the reverse circulation sampling, outlet sampling, coring tube sampling, and the sealed coring, as shown in Fig. 11(c) and (d) (data from previous studies (Jing, 2015; Zhang H. et al., 2021; Wang et al., 2013; Wang et al., 2020; Zheng et al., 2015; Zhang, 2019; Kang, 2017).

5.4. Theoretical model of optimal coring depth in in situ coal seams

The prerequisite for accurately determining the in-situ gas content of regional coal seams is to determine the optimal coring depth. When the coring depth is short, the measured gas content is greatly affected by engineering disturbances and does not represent the regional in-situ gas content. On the other hand, if the coring depth is too long, it will result in extra economic cost and resource wastage at the coal mine site. Therefore, to facilitate each mine in determining the optimal coring depth based on the geological conditions and engineering characteristics of the sampling area, a calculation method is proposed to determine the optimal coring depth for measuring the in-situ gas content of coal seams. To facilitate on-site applications, it is necessary to establish corresponding theoretical models for practical use.

The study established a coordinate system as shown in Fig. 12, with the direction of the x-axis represents the drilling direction, and x represents the straight-line distance from a certain point within the coal seam to the roadway wall. Assuming ρ is density of the coal seam, h is thickness of the coal seam, L is depth of the gas desorption affected zone under engineering disturbance, and W is original gas content of the coal seam, the total gas content of the coal within the range of engineering disturbances, including roadway excavation, adjacent coal seam mining, and core drilling, can be calculated using Eq. (20).

$$\chi = \rho hLW \tag{20}$$

The gas outflow within the disturbance range during the process of roadway excavation and coring drilling is given by Eq. (21),

$$\chi_d = \int_0^t Vc(t)\mathrm{d}t \tag{21}$$

where V is the volume enclosed by the research area, which consists of the roadway and the surrounding coal seam. The research area is set as a two-dimensional plane, and the width of the roadway is denoted as b. Therefore, $V = bh$, as shown in Eq. (22).

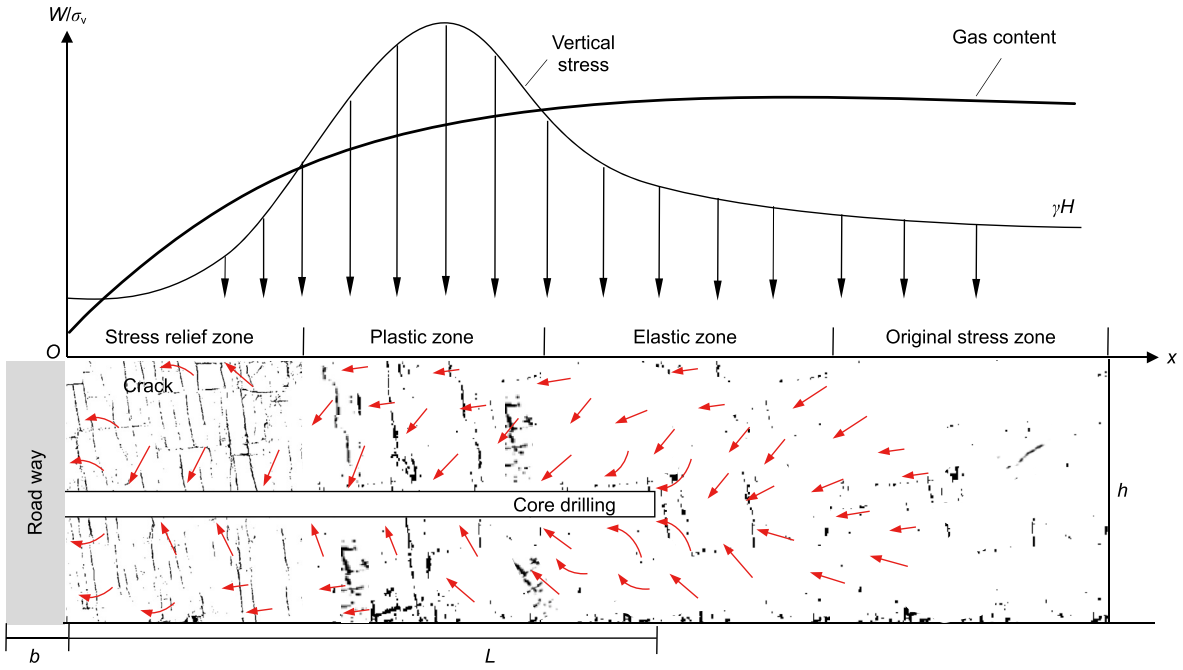

Fig. 12. Schematic diagram of stress and gas content distribution around the drilling borehole in coal seam (the black trace represents the crack/fracture, the red arrow represents the direction of gas flow; the stress relief area corresponds to area A in Fig. 5, the plastic zone and the elastic area correspond to area B in Fig. 5, and the original rock stress area corresponds to area C in Fig. 5.).

$$\chi_d = bh\int_0^t c(t)\mathrm{d}t \tag{22}$$

The time refers to the total time from roadway excavation to completion of coring drilling, i.e., the tunneling time. The $c(t)$ represents the average gas concentration released from the coal within the research range, which is a function of time. According to the law of mass conservation, the total gas amount (measured by volume) within the disturbed coal body is equal to the sum of the released gas amount and the residual gas amount, as shown in Eq. (23).

$$\chi = \chi_d + \chi_r \tag{23}$$

In Eq. (23), if the desorption hysteresis effects is not considered (Chu et al., 2023, 2024), χ represents the total gas amount of the coal seam, χ_r represents the gas amount released during the core drilling process, and χ_d represents the residual gas amount of the coal seam.

The residual gas amount of the coal seam (measured by volume) is given by Eq. (24).

$$\chi_r = \int_0^L\int_0^t W_r(x,t)\mathrm{d}t\mathrm{d}x \tag{24}$$

The residual gas content $W_r(x, t)$ within the research area of the coal seam varies in both temporal and spatial dimensions due to the influence of mining activities, such as the stress state and gas geological conditions.

Based on mass conservation, it is assumed that all gas desorbed by coal seams diffuses through pores, seeps into the mining space, and leaves the coal seam with mine ventilation. The influence of environmental factors such as temperature and coal seam moisture content on gas migration is not considered. This study analyzes the gas migration process from a time series perspective, and defines $R^c(x,t)$ to represent the residual gas amount of the target coal seam at time t at x position from the tunnel wall, which gradually decreases with time, m^3/t or cm^3/g; The parameter $D^e(x,t)$ represents the natural desorption rate of gas in the coal seam at time t at a distance x from the tunnel wall, i.e., the ratio of the gas desorption amount per unit time (cm^3/g) to the in-situ gas content, which gradually increases over time without considering the negligible change of geological environmental conditions of the coal, $cm^3\cdot min^{-1}$;

The parameter $D^s(x,t)$ represents the gas diffusion and seepage rate in the coal seam at time t, that is, the ratio of the gas migration amount to the gas desorption amount per unit time, $cm^3\cdot min^{-1}$; The constant a is a parameter related to the physical properties such as pore connectivity and pore structure of the coal body; initial condition: $t = 0$ time, $R_0 = R^c(x, 0)$, which is the original gas content.

If this gas migration process is investigated within a short period of time $[t, t + \Delta t]$, the change in the amount of residual gas in the coal seam can be approximately described by the difference Eq. (25):

$$\Delta R^c = D^e(x\ ,\ t)\cdot R^c(x,t)\Delta t - D^s(x,t)\cdot R^c(x,t)\Delta t \tag{25}$$

So that:

$$\Delta R^c = \left[D^e(x\ ,\ t) - D^s(x,t)\right]R^c(x,t)\Delta t \tag{26}$$

Therefore, its differential Eq. (27) is in the form:

$$\frac{\mathrm{d}R^c(x,t)}{\mathrm{d}t} = \left[D^e(x,t) - D^s(x,t)\right]R^c(x,t) \tag{27}$$

Under specific geological environmental conditions, the gas desorption and migration rates in coal seams are relatively constant and can be regarded as constants. therefore:

$$R^c(x,t) = R_0^c\mathrm{e}^{[D^e(x,t)-D^s(x,t)]t} \tag{28}$$

And,

$$D^e(x,t) - D^s(x,t) = \frac{a(W_0 - R)}{W_0} \tag{29}$$

Thus,

$$R^c(x,t) = R_0^c\mathrm{e}^{\frac{a(W_0-R)}{W_0}} \tag{30}$$

$$R^c(x,t) = \frac{W_0}{1 + \frac{W_0-R_0^c}{R_0}\mathrm{e}^{-at}} \tag{31}$$

And, $0 < R_0 < W_0$.

By substituting Eqs. (22) and (24) into Eq. (23), and combining Eqs. (20) and (23) based on the law of mass conservation, Eq. (32) can be obtained.

$$\rho hLW = \int_0^t bhc(t)\mathrm{d}t + \int_0^L\int_0^t W_r(x,t)\mathrm{d}t\mathrm{d}x \tag{32}$$

Thus, the depth of the gas desorption affected zone under engineering disturbance can be calculated and predicted employing Eq. (33)

$$L = \frac{1}{\rho hW}\left(bh\int_0^t c(t)\mathrm{d}t + \int_0^L\int_0^t W_r(x,t)\mathrm{d}t\mathrm{d}x\right) \tag{33}$$

In summary, by comprehensive comparison of permeability simulation results, distribution law of borehole surrounding rock fractures and field test data of gas content, the gas distribution law of coal seam surrounding the borehole has obvious zoning phenomenon under different coring depths, and the coring depth should be greater than the area affected by roadway excavation and drilling disturbance. Therefore, according to the field conditions of the model in this study, it is recommended that the coring depth should be greater than 17 m. At the same time, in the subsequent research, it is useful to further carry out comprehensive impact research on the affected area of excavation disturbance, the sampling time of pressure and gas preservation and core depth, and further explore the scientific nature of sampling process optimization.

Through a comprehensive comparative analysis of the distribution patterns of stress and permeability of the surrounding rock on the side walls of the tunnel in the literature, as the sampling depth increases, the stress and permeability of the surrounding

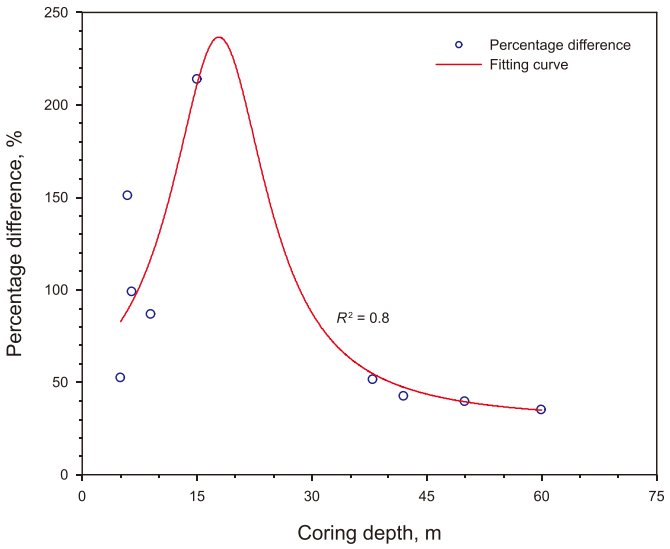

Fig. 13. Gas content measured in the field tests with different coring depths in coal seam.

rock of the tunnel have obvious zoning characteristics. Due to the differences in the mechanical properties and stress distribution of the surrounding rock in each mining area. As a result, there are slight differences in the specific partitions of stress, but the overall pattern is consistent with the results calculated in this study, as shown in Fig. 13. At the same time, to further reveal the distribution pattern of in-situ gas content in the coal seam surrounding the roadway, the gas content was measured using the pressure-preserved coring technique at different sampling depths of the coal seam, as shown in Table 3. The measurement results showed that there was gas content threshold about 17 m away from the roadway surrounding rock. The threshold value is that within the sampling depth of 17 m, the gas content gradually increases as the sampling depth increases; after the sampling depth is greater than 17 m, the relationship between the gas content and the sampling depth gradually weakens. The drilling depth where this threshold exists is the optimal sampling depth. If the gas content in a certain area of the coal seam is to be measured, the sampling depth should be at least great than 17 m. At the same time, it should be noted that the gas content results obtained by using the pressure-preserved coring technique in this study are from two mining areas. The sampling depth less than 30 m is one type of mining area, and the sampling depth greater than 30 m is another type of mining area. Therefore, the differences in the coal seams themselves may lead to differences in the gas content measurement results of the two mining areas, but it does not affect the conclusion of this study on the relationship between the gas content measurement results and sampling depth.

6. Conclusions

A model is constructed and coupled with multi-physics and considers the influence of roadway and borehole excavation disturbance on gas migration. The model can predict the in-situ gas occurrence law under different coring depths according to different geological conditions. The combined method of FLAC^{3D} and COMSOL is innovatively adopted. This method combines the advantages of the two kinds of software to further improve the accuracy and efficiency of coal-rock gas migration under the background of large displacement and large deformation.

(1) The reliability of the model is verified by on-site borehole inspection and downhole gas content measurement results. The roadway surrounding coal seam exhibits zoning characteristics after excavation, including stress relief zone, stress concentration zone that is composed of plastic zone, elastic zone, and original stress zone. The vertical stress, permeability, gas pressure, gas content distribution, and borehole wall breakage align with the simulated partition characteristics.

(2) Based on comprehensive analyses of the surrounding rock drilling images, the distribution of gas content, vertical stress, permeability, and gas pressure at different coring depths, and considering the drilling disturbance and roadway excavation time, the study proposes a set of drilling and coring depth calculation and prediction model for the gas desorption affected area under engineering disturbance; and if the roadway excavation time is ~1 year, the recommended coring depth for a typical coal seam similar to the study should be at least 17 m.

(3) By comparing and analyzing the differences between the traditional gas content measurement method and the pressure-preserved gas coring with integrated transfer test method, an in-situ gas measurement process for coal seams is proposed for underground coal mines. These findings offer valuable theoretical guidance for operating in-situ pressure-preserved coring in a variety of conditions.

CRediT authorship contribution statement

Peng-Fei Cui: Writing – original draft, Investigation. **De-Lei Shang:** Writing – review & editing, Visualization, Supervision, Investigation, Funding acquisition, Data curation. **Peng Chu:** Software, Methodology. **Ju Li:** Validation, Data curation. **Da-Li Sun:** Methodology, Conceptualization. **Tian-Yu Wang:** Validation. **Ming-Zhong Gao:** Supervision, Resources, Project administration, Funding acquisition. **He-Ping Xie:** Supervision, Resources, Project administration, Funding acquisition.

Declaration of competing interest

The authors declare that they have no known competing financial interests or personal relationships that could have appeared to influence the work reported in this paper.

Acknowledgements

The study is supported by National Natural Science Foundation of China (Nos. 51827901, 52104096), the Shenzhen National Science Fund for Distinguished Young Scholars (No. RCJC20210706091948015), Open Fund of State Key Laboratory of Hydraulics and Mountain River Engineering, Sichuan University (No. SKHL2216), National Key R & D Program of China (No. 2022YFB3706605), Youth Foundation of Sichuan Natural Science Foundation (No. 2023NSFSC0780).

Appendix A

Symbol	Meaning	Symbol	Meaning
c	Cohesion, MPa	p_f	Gas pressure in fracture, MPa
c_0	The initial cohesion, MPa	α	One of the key parameters in gas flow model which affects the rate of matrix gas diffusing into cleat system
c_1	The residual cohesion, MPa	τ	The sorption time of the coal matrix
γ^p	Softening parameter	m_f	Quantity of free gas in fracture per volume of coal, kg
γ^{p*}	Critical softening parameter from which the residual stage begins.	ρ_f	The density of gas in fracture, kg/m^3
ε_1^p, ε_2^p, ε_3^p	Plastic strain increments	v_f	Gas flow velocity in fractures, m/s
δ	Plastic multiplier	φ_f	The fracture porosity, %
m_m	Methane mass per volume of coal matrix, kg/m^3	k	Permeability, m^2
Q_S	Methane mass exchange rate between matrix and fracture per volume of coal, kg/(m^3·s)	μ	Kinetic viscosity of methane
V_L	Langmuir volume constant, m^3/kg	k_0	The initial permeability of coal, m^2
p_L	Langmuir pressure constant, MPa	ε_V	The volume strain of coal
p_m	Gas pressure in matrix, MPa	φ_{f0}	Initial porosity of fractures
M_C	Molar mass of the methane, kg/mol	ν	Poisson ratio
V_M	Molar volume of the methane under standard conditions, 0.0224 m^3/mol	E	Young's modulus of coal body
ρ_C	Apparent density of coal, kg/m^3	α_m, α_f	Effective stress coefficients of pores and fractures
R	Universal gas constant, J/(mol·K)	p_{m0}, p_{f0}	Initial pressure of gas pressure in matrixes and fractures
T	Temperature, K	ε_L	Maximum strain induced by sorption
φ_m	Matrix porosity		

References

Chu, P., Shang, D., Li, J., et al., 2023. Influence of gas components on the determination of gas pressure in coal seams under in-situ pressure-preserved coring. Meitiandizhi Yu Kantan/Coal Geology and Exploration. 51 (8), 79–87. https://doi.org/10.12363/issn.1001-1986.22.12.0939 (in Chinese).

Chu, P., Xie, H., Gao, M., et al., 2024. Influence of desorption hysteresis effects on coalbed methane migration and production based on dual-porosity medium model incorporating hysteresis pressure. Comput. and Geotech. 165, 105893. https://doi.org/10.1016/j.compgeo.2023.105893.

Cui, P., Gao, M., Shang, D., et al., 2023. A preliminary study of pressure-preserved coring calculation principle and method for in-situ pressure in deep coal seams. Meitiandizhi Yu Kantan/Coal Geology and Exploration. 51 (8), 59–67. https://doi.org/10.12363/issn.1001-1986.22.12.0934 (in Chinese).

Gao, M., Chen, L., Fan, D., et al., 2021. Principle and technology of coring with in-situ pressure and gas maintaining in deep coal mine. J. China Coal Soc. 46 (3), 885–897. https://doi.org/10.13225/j.cnki.jccs.YT21.0297 (in Chinese).

Gao, M.Z., Jin, W.C., Zheng, C.J., et al., 2012. Real-time evolution and connectivity of mined crack network. J. China Coal Soc. 37 (9), 1535–1540. https://doi.org/10.13225/j.cnki.jccs.2012.09.023 (in Chinese).

Gao, M.Z., Liu, J.J., Lin, W.M., et al., 2020. Study on in - situ stress evolution law of ultra - thick coal seam in advance mining. Coal Sci. Technol. 48 (2), 28–35. https://doi.org/10.13199/j.cnki.cst.2020.02.003 (in Chinese).

Hao, F.C., Wei, L.Y., Cheng, L.W., et al., 2017. Effective gas extraction radius of different burial depths under creep- seepage coupling. J. China Coal Soc. 42 (10), 2616–2622. https://doi.org/10.13225/j.cnki.jccs.2017.0459 (in Chinese).

Harrison, J., Hudson, J., Popescu, M., 2002. Engineering rock mechanics: Part 2. Illustrative worked examples. Appl. Mech. Rev. 55 (2), B30–B31. https://doi.org/10.1115/1.1451165.

He, M.C., Xie, H.P., Peng, S.P., et al., 2005. Study on rock mechanics in deep mining engineering. Yanshilixue Yu Gongcheng Xuebao/Chinese Journal of Rock Mechanics and Engineering 24 (16), 2803–2813. https://doi.org/10.3321/j.issn:1000-6915.2005.16.001 (in Chinese).

Huang, W., Chen, L., Li, J., et al., 2023a. R&D and experimental research of pressure-preserved triggering device for horizontal pressure-preserved coring in coal mines. Meitiandizhi Yu Kantan/Coal Geology and Exploration 51 (8), 39–46. https://doi.org/10.12363/issn.1001-1986.22.12.0933 (in Chinese).

Huang, W., Li, J., Liu, Z., et al., 2023b. Study of a low-disturbance pressure-preserving corer and its coring performance in deep coal mining conditions. Int. J. Min. Sci. Technol. 33 (11), 1397–1410. https://doi.org/10.1016/j.ijmst.2023.07.003.

Hungerford, F., Ren, T., 2014. Directional drilling in unstable environments. Int. J. Min. Sci. Technol. 24 (3), 397–402. https://doi.org/10.1016/j.ijmst.2014.03.019.

Jiang, Y.D., Liu, W.G., Zhao, Y.X., et al., 2005. Study on surrounding rock stability of deep mining in kailuan mining group. Chin. J. Rock Mech. Eng. 24 (11), 1857–1862. https://doi.org/10.3321/j.issn:1000-6915.2005.11.007 (in Chinese).

Jing, X., 2015. Study on integrate technique of mechanical sealed coring and methane content measuring. Journal of Safety Science and Technology 11 (11), 59–63. https://doi.org/10.11731/j.issn.1673-193x.2015.11.010 (in Chinese).

Kang, J., 2017. Study of Reverse Circulation Sampling Method Applied in Underground on Site Measurements for Coal Seam Gas Content. Ph.D. Thesis. Shandong University of Science and Technology, Qingdao. https://doi.org/10.27275/d.cnki.gsdku.2017.000008 (in Chinese).

Liang, B., Zhang, M.T., Wang, Y.J., 1996. Mathematical model and numerical method for coupled gas flow in coal seams and coal deformation. Chin. J. Rock Mech. Eng. 15 (2), 40–47 (in Chinese).

Liang, W., Li, C., Liu, G., et al., 2023. Pressure-bearing characteristics of pressure-preserved controllers under deep in-situ temperature and pressure conditions. Meitiandizhi Yu Kantan/Coal Geology and Exploration. 51 (8), 68–78. https://doi.org/10.12363/issn.1001-1986.23.07.0407 (in Chinese).

Liu, G., Li, C., You, Z., et al., 2023. Principle and technology of in-situ magnetically controlled multidirectional pressure-preserved coring in the coal mine. Meitiandizhi Yu Kantan/Coal Geology and Exploration. 51 (8), 13–20. https://doi.org/10.12363/issn.1001-1986.22.12.0935 (in Chinese).

Liu, Q., Chu, P., Zhu, J., et al., 2020. Numerical assessment of the critical factors in determining coal seam permeability based on the field data. J. Nat. Gas Sci. Eng. 74, 103098. https://doi.org/10.1016/j.jngse.2019.103098.

Long, W.C., Sun, S.Q., 2021. Research on wireline sealed coring equipment and technology for coalbed methane content determination. Coal Geol. Explor. 49 (3), 133–139. https://doi.org/10.3969/j.issn.1001-1986.2021.03.017 (in Chinese).

Luo, C., Li, H., Liu, Y., 2010. Study of distributing characteristics of stress in surrounding rock masses and in-situ stress measurement for deeply buried tunnels. Yanshilixue Yu Gongcheng Xuebao/Chinese Journal of Rock Mechanics and Engineering 29 (7), 1418–1423 (in Chinese).

Martino, J.B., Chandler, N.A., 2004. Excavation-induced damage studies at the underground research laboratory. Int. J. Rock Mech. Min. Sci. 41 (8), 1413–1426. https://doi.org/10.1016/j.ijrmms.2004.09.010.

Meng, B., Jing, H., Chen, K., et al., 2013. Failure mechanism and stability control of a large section of very soft roadway surrounding rock shear slip. Int. J. Min. Sci. Technol. 23 (1), 127–134. https://doi.org/10.1016/j.ijmst.2013.03.002.

Pourhosseini, O., Shabanimashcool, M., 2014. Development of an elasto-plastic constitutive model for intact rocks. Int. J. Rock Mech. Min. Sci. 66 (66), 1–12. https://doi.org/10.1016/j.ijrmms.2013.11.010.

Qi, L.M., Chen, X.X., Cheng, W.Y., et al., 2010. Newly deveolped method for exact measurement of gas content. Journal of Mining & Safety Engineering 27 (1), 111–115. https://doi.org/10.3969/j.issn.1673-3363.2010.01.021 (in Chinese).

Shi, X., Li, M., Liu, G., et al., 2023. Simulation optimization and applications of pressure-preserved triggering device for coring in deep coal mines. Meitiandizhi Yu Kantan/Coal Geology and Exploration 51 (8), 21–29. https://doi.org/10.12363/issn.1001-1986.22.12.0936 (in Chinese).

Sun, S., Zhang, Q., Zheng, K., et al., 2020. Technology and equipment of sealed coring for accurate determination of coalbed gas content in ground well. J. China Coal Soc. 45 (7), 2523–2530. https://doi.org/10.13225/j.cnki.jccs.DZ20.0672 (in Chinese).

Tu, Q.Y., Cheng, Y.P., Liu, Q.Q., et al., 2018. Investigation of the formation mechanism

of coal spallation through the cross-coupling relations of multiple physical processes. Int. J. Rock Mech. Min. Sci. 105, 133–144. https://doi.org/10.1016/j.ijrmms.2018.03.022.

Wang, D., Tang, J., Wei, J., et al., 2023. A fluid-solid coupling model of coal seam gas considering gas multi-mechanism flow and a numerical simulation analysis of gas drainage. Meitan Xuebao/Journal of the China Coal Society 48 (2), 763–775. https://doi.org/10.13225/j.cnki.jccs.2022.0853 (in Chinese).

Wang, E.Y., Liu, S.Q., Gao, R.B., et al., 2017. Transient electromagnetic exploration-based experiment on the relationship between the level of gas content and apparent resistivity in high rank coal seam. Coal Geol. Explor. 45 (6), 149–153. https://doi.org/10.3969/j.issn.1001-1986.2017.06.024 (in Chinese).

Wang, G., Xie, J., Duan, Y., et al., 2013. Direct method of determining gas content of coal beds from clastic coal core. Caikuang yu Anquan Gongcheng Xuebao/Journal of Mining and Safety Engineering 30 (4), 610–615 (in Chinese).

Wang, L., Wang, Z.F., Qi, C.J., et al., 2019. Physical simulation of temperature and pressure evolvement in coal by different refrigeration modes for freezing coring. ACS Omega 4 (23), 20178–20187. https://doi.org/10.1021/acsomega.9b02333.

Wang, M., Sun, Y., Hao, F., 2020. Research on pre-drainage gas equivalent width of roadway under seepage-stress coupling. Coal Sci. Technol. 48 (12), 109–115. https://doi.org/10.13199/j.cnki.cst.2020.12.013 (in Chinese).

Wang, T., Li, J., Zhang, Y., et al., 2023. Sealing performance analysis and structure optimization of pressure-preserved controller for pressure-preserved coring in deep coal mine. Meitiandizhi Yu Kantan/Coal Geology and Exploration. 51 (8), 88–97. https://doi.org/10.12363/issn.1001-1986.22.12.0961 (in Chinese).

Wei, P., Guo, C.Y., Zhao, S., et al., 2019. Determination of appropriate sampling depth of coalbed gas content: a case study. J. Geophys. Eng. 16 (2), 411–422. https://doi.org/10.1093/jge/gxz018.

Wen, Z.H., Zhang, H.T., Wei, J.P., et al., 2017. Gas loss calculation method for gas content determination by sampling method based on negative pressure pneumatic conveying. J. China Univ. Min. Technol. 46 (4), 776–782. https://doi.org/10.13247/j.cnki.jcumt.000706 (in Chinese).

Xiao, X.C., Pan, Y.S., 2005. Mathematical model and numerical simulation of coalbed methane percolation flow equation considering slippage effects. Chin. J. Rock Mech. Eng. 24 (16), 2966–2970. https://doi.org/10.3321/j.issn:1000-6915.2005.16.026 (in Chinese).

Xie, H., Cui, P., Shang, D., et al., 2023. Research advances on the in-situ pressure-preserved coring and gas parameter determination for deep coal seams. Meitiandizhi Yu Kantan/Coal Geology and Exploration, 51 (8), 1–12. https://doi.org/10.12363/issn.1001-1986.23.02.0075 (in Chinese).

Xie, H., Gao, M., Fu, C., et al., 2021. Mechanical behavior of brittle-ductile transition in rocks at different depths. Meitan Xuebao/Journal of the China Coal Society 46 (3), 701–715. https://doi.org/10.13225/j.cnki.jccs.YT21.0157 (in Chinese).

Xie, H., Gao, M., Zhang, R., et al., 2020. Study on concept and progress of in situ fidelity coring of deep rocks. Yanshilixue Yu Gongcheng Xuebao/Chinese Journal of Rock Mechanics and Engineering 39 (5), 865–876. https://doi.org/10.13722/j.cnki.jrme.2020.0138 (in Chinese).

Xie, H., Gao, F., Zhou, H., et al., 2013. On theoretical and modeling approach to mining-enhanced permeability for simultaneous exploitation of coal and gas. J. China Coal Soc. 38 (7), 1101–1108. https://doi.org/10.13225/j.cnki.jccs.2013.07.016 (in Chinese).

Xue, S., Yuan, L., 2017. The use of coal cuttings from underground boreholes to determine gas content of coal with direct desorption method. Int. J. Coal Geol. 174, 1–7. https://doi.org/10.1016/j.coal.2017.03.007 (in Chinese).

Xue, Y., Gao, F., Liu, X., et al., 2017. Permeability and pressure distribution characteristics of the roadway surrounding rock in the damaged zone of an excavation. Int. J. Min. Sci. Technol. 27 (2), 211–219. https://doi.org/10.1016/j.ijmst.2017.01.003.

Yan, X.W., 2021. Research on large deformation mechanism and repair support technology of high stress soft rock roadway. Ind. Mine Autom. 47 (6), 116–123. https://doi.org/10.13272/j.issn.1671-251x.2021010007.

Yao, S., 2022. Research on the Effect of Grouting Plugging and Seepage Reduction in Fractured Coal Body and the Application of Drainage Drilling and Sealing. Master's Thesis. Henan Polytechnic University, Jiaozhuo. https://doi.org/10.27116/d.cnki.gjzgc.2022.000671 (in Chinese).

Yin, G., Li, M.H., Li, S.Z., et al., 2013. 3D numerical simulation of gas drainage from boreholes based on solid-gas coupling model of coal containing gas. J. China Coal Soc. 38 (4), 535–541. https://doi.org/10.13225/j.cnki.jccs.2013.04.012 (in Chinese).

Yin, G., Wang, D., Zhang, D., et al., 2008. Solid-gas coupling dynamic model and numerical simulation of coal containing gas. Chin. J. Geotech. Eng. (10), 1430–1436. https://doi.org/10.3321/j.issn:1000-4548.2008.10.002 (in Chinese).

Yuan, Y., Zhu, Y., Wang, W., et al., 2014. Failure mechanism of Mesozoic soft rock roadway in Shajihai coal mine and its surrounding rock control. Int. J. Min. Sci. Technol. 24 (6), 853–858. https://doi.org/10.1016/j.ijmst.2014.10.019.

Zhang, C.L., Wang, E.Y., Xu, J., et al., 2021. The influence of coal seam gas pressure on gas drainage effect. Journal of Mining & Safety Engineering 39 (3), 1–12. https://doi.org/10.13545/j.cnki.jmse.2021.0189 (in Chinese).

Zhang, H., Cheng, Y.P., Deng, C.B., et al., 2021. A novel in-seam borehole discontinuous hydraulic flushing technology in the driving face of soft coal seams: enhanced gas extraction mechanism and field application. Rock Mech. Rock Eng. 55 (2), 885–907. https://doi.org/10.1007/s00603-021-02691-w.

Zhang, R., 2019. Cutting test of coal with different hardness by reverse circulation sampling bit. Saf. Coal Mine 50 (2), 95–98. https://doi.org/10.13347/j.cnki.mkaq.2019.02.021 (in Chinese).

Zhang, S., 2021. Absorbent Bag Type Horizontal Drilling and Sealing Technology and its Application in the Study of the Width of Stress-Relief Zone of the Coal Body beside Tunnel. Master's Thesis. Xuzhou: China University of Mining and Technology. https://doi.org/10.27623/d.cnki.gzkyu.2021.001529 (in Chinese).

Zhao, W., Wang, K., Ju, Y., et al., 2020. Influence of the roadway exposure time on the accuracy of gas content measurements in reconstructed and extended mines. Process Saf. Environ. Protect. 142, 109–117. https://doi.org/10.1016/j.psep.2020.06.016.

Zheng, P., Wang, J., Xue, S., et al., 2015. Effect of different sampling depth in the same seam on the measured value of gas content. Coal Engineering 47 (7), 101–103+106. https://doi.org/10.11799/ce201507033 (in Chinese).

Zhou, H., Kun, Q.C., Wang, Z.C., et al., 2017. Simulating the variation of surrounding rock and analyzing the disturbed stress field during excavation of deep mine roadway. Chin. J. Rock Mech. Eng. 36 (8), 1821–1831. https://doi.org/10.13722/j.cnki.jrme.2017.0026 (in Chinese).

Zhu, P., Li, J., Li, J., et al., 2023. Development of self-locking transfer mechanism for coal samples from pressure-preserved coring in deep mining. Meitiandizhi Yu Kantan/Coal Geology and Exploration. 51 (8), 47–58. https://doi.org/10.12363/issn.1001-1986.23.01.0027 (in Chinese).

Zou, Y.H., Zhang, Q.H., 2009. Technical progress of direct determination of gas content in coal mines in China. Mining Safety &amp. Environ. Protect. 36 (S1), 180–182. https://doi.org/10.3969/j.issn.1008-4495.2009.z1.066 (in Chinese).